AD-A065 090 ARMY ENGINEER WATERWAYS EXPERIMENT STATION VICKSBURG MISS F/G 8/8
A NUMERICAL MODEL FOR TSUNAMI INUNDATION.(U)
FEB 79 J R HOUSTON, H L BUTLER

UNCLASSIFIED WES-TR-HL-79-2 NL

1 OF 1
ADA
065090

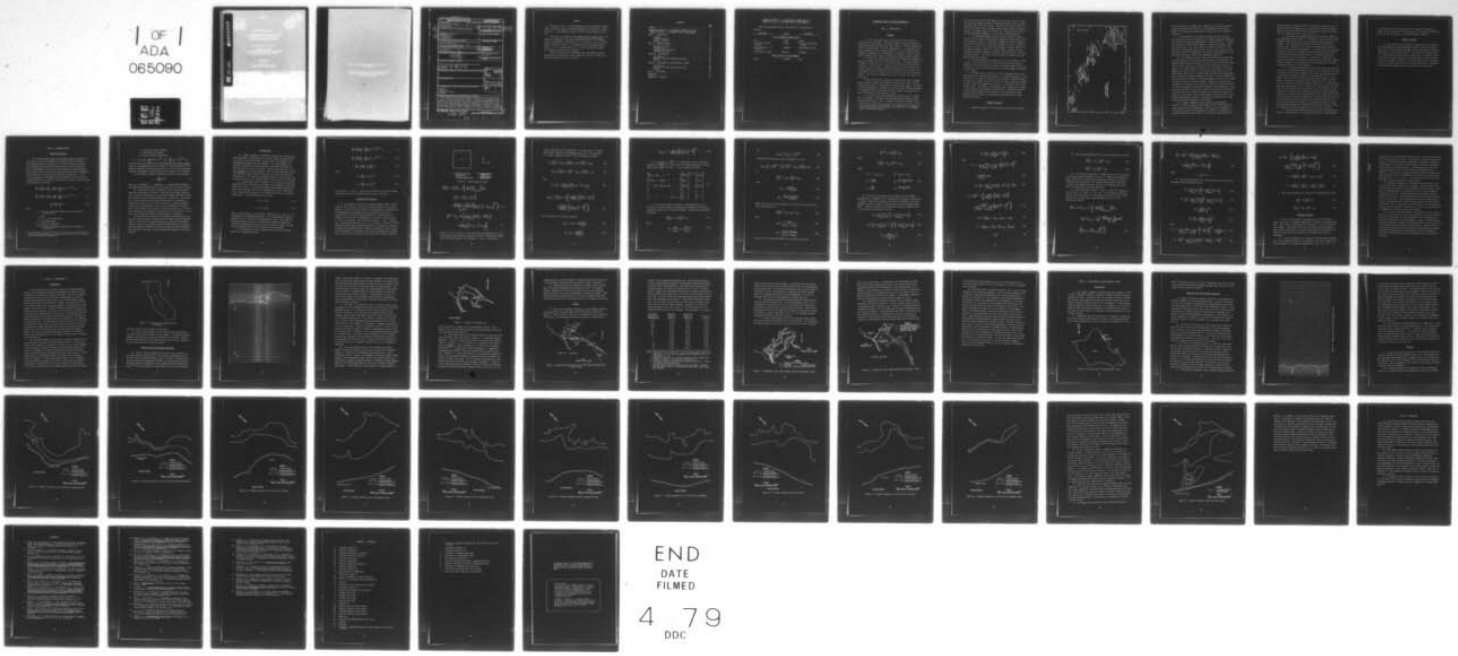

END
DATE
FILMED
4 79
DDC

Unclassified

SECURITY CLASSIFICATION OF THIS PAGE (When Data Entered)

REPORT DOCUMENTATION PAGE

READ INSTRUCTIONS BEFORE COMPLETING FORM

1. REPORT NUMBER: Technical Report HL-79-2
2. GOVT ACCESSION NO.:
3. RECIPIENT'S CATALOG NUMBER:

4. TITLE (and Subtitle): A NUMERICAL MODEL FOR TSUNAMI INUNDATION.

5. TYPE OF REPORT & PERIOD COVERED: Final report. Nov 77—Oct 78

6. PERFORMING ORG. REPORT NUMBER:

7. AUTHOR(s): James R. Houston, H. Lee Butler

8. CONTRACT OR GRANT NUMBER(s):

9. PERFORMING ORGANIZATION NAME AND ADDRESS:
U. S. Army Engineer Waterways Experiment Station
Hydraulics Laboratory
P. O. Box 631, Vicksburg, Miss. 39180

10. PROGRAM ELEMENT, PROJECT, TASK AREA & WORK UNIT NUMBERS:

11. CONTROLLING OFFICE NAME AND ADDRESS:
U. S. Army Engineer Division, Pacific Ocean
Building 230
Fort Shafter, Hawaii 96858

12. REPORT DATE: February 1979

13. NUMBER OF PAGES: 56

14. MONITORING AGENCY NAME & ADDRESS (if different from Controlling Office): 64p.

15. SECURITY CLASS. (of this report): Unclassified

15a. DECLASSIFICATION/DOWNGRADING SCHEDULE:

16. DISTRIBUTION STATEMENT (of this Report)

Approved for public release; distribution unlimited.

WES-TR-HL-79-2

17. DISTRIBUTION STATEMENT (of the abstract entered in Block 20, if different from Report)

18. SUPPLEMENTARY NOTES

19. KEY WORDS (Continue on reverse side if necessary and identify by block number)

Floods
Long waves
Mathematical models
Tsunamis

20. ABSTRACT (Continue on reverse side if necessary and identify by block number)

A two-dimensional and time-dependent numerical model was developed that calculates the land inundation of a tsunami. The model solves long wave equations that include bottom friction terms. A coordinate transformation was used to allow the model to employ a smoothly varying grid that allows cells to be small in the inundation region and large in the ocean. The model was verified by simulating the 1964 Alaskan tsunami at Crescent City, California. An application of the model to calculate inundation in a region of Hawaii is presented.

ACCESSION for
NTIS White Section
DDC Buff Section
UNANNOUNCED
JUSTIFICATION
BY
DISTRIBUTION/AVAILABILITY CODES
Dist. AVAIL. and/or SPECIAL

DD FORM 1 JAN 73 1473 EDITION OF 1 NOV 65 IS OBSOLETE

Unclassified

SECURITY CLASSIFICATION OF THIS PAGE (When Data Entered)

038 100

PREFACE

Authority for the U. S. Army Engineer Waterways Experiment Station (WES) to conduct a study of tsunami inundation was contained in a letter from the U. S. Army Engineer Division, Pacific Ocean, dated 26 October 1977.

This study was conducted from November 1977 to October 1978 in the Hydraulics Laboratory, WES, under the direction of Mr. H. B. Simmons, Chief of the Hydraulics Laboratory, Dr. R. W. Whalin, Chief of the Wave Dynamics Division, and Mr. D. D. Davidson, Chief of the Wave Research Branch. Dr. J. R. Houston and Mr. H. L. Butler conducted the study. This report was prepared by Dr. Houston.

Commander and Director of WES during the investigation and the preparation and publication of this report was COL John L. Cannon, CE. Technical Director was Mr. F. R. Brown.

CONTENTS

CONVERSION FACTORS, U. S. CUSTOMARY TO METRIC (SI) AND METRIC (SI) TO U. S. CUSTOMARY UNITS OF MEASUREMENT

Units of measurement used in this report can be converted as follows:

Multiply	By	To Obtain
U. S. Customary to Metric (SI)		
feet	0.3048	metres
feet per second per second	0.3048	metres per second per second
miles per hour (U. S. statute)	1.609344	kilometres per hour
tons (2,000 lb, mass)	907.1847	kilograms
Metric (SI) to U. S. Customary		
metres	3.280839	feet

A NUMERICAL MODEL FOR TSUNAMI INUNDATION

PART I: INTRODUCTION

Tsunamis

1. Of all water waves that occur in nature, one of the most destructive is the tsunami. The term "tsunami," originating from the Japanese words "tsu" (harbor) and "nami" (wave), is used to describe sea waves of seismic origin. Tectonic earthquakes, i. e. earthquakes that cause a deformation of the seabed, appear to be the principal seismic mechanism responsible for the generation of tsunamis. Coastal and submarine landslides and volcanic eruptions also have triggered tsunamis.

2. Tsunamis are principally generated by undersea earthquakes of magnitudes greater than 6.5 on the Richter scale. The typical height of a tsunami in the deep ocean is less than a foot and the wave period is 5 minutes to several hours. Tsunamis travel at the shallow-water wave celerity equal to the square root of acceleration due to gravity times water depth even in the deepest oceans because of their very long wavelengths. This speed of propagation can be in excess of 500 mph* in the deep ocean.

3. When tsunami waves approach a coastal region where the water depth decreases rapidly, wave refraction, shoaling, and bay or harbor resonance may result in significantly increased wave heights. The great period and wavelength of tsunami waves preclude their dissipating energy as a breaking surf; instead, they are apt to appear as rapidly rising water levels and only occasionally as bores.

4. The loss of life and destruction of property due to tsunamis have been immense. The Great Hoei Tokaido-Nanhaido tsunami of Japan killed 30,000 people in 1707. In 1868, the Great Peru tsunami caused

---

* A table of factors for converting U. S. customary units of measurement to metric (SI) units and metric (SI) units to U. S. customary units is presented on page 3.

25,000 deaths and carried the frigate U.S.S. Waterlee 1,300 ft inland. The Great Meiji Sanriku tsunami of 1896 killed 27,122 persons in Japan and washed away over 10,000 houses. The most recent major tsunami to affect the United States, the 1964 Alaskan tsunami, killed 107 people in Alaska, 4 in Oregon, and 11 in Crescent City, California, and caused over $100 million in damage on the west coast of North America.[1]

5. The Hawaiian Islands, a chain of eight islands as shown in Figure 1, have a history of destructive tsunamis generated both in distant areas and locally. The earliest recording of a severe tsunami in the Hawaiian Islands was in 1837 when a tsunami from Chile reached an elevation of 20 ft at Hilo and killed 46 people in the Kau District of the island of Hawaii (Figure 1). Prior to 1837, a number of severe tsunamis undoubtedly reached the islands, but unfortunately no detailed records were kept. Since 1837, there have been 16 tsunamis that have caused significant damage.[2]

6. The most destructive tsunami to ever hit the islands in terms of loss of life and destruction of property was the Great Aleutian tsunami of 1946, which killed 173 people and produced waves over 55 ft in elevation. Hilo incurred $26 million in property damage attributable to this tsunami.

7. The 1960 Chilean tsunami is the most recent distantly generated tsunami that produced major effects in the Hawaiian Islands. Sixty-one lives, all at Hilo, were claimed by the tsunami. Damage throughout the State was estimated to be $23.5 million of which 93 percent occurred at Hilo. Other major damage was restricted to the Kahului area of the Island of Maui. Inspection of the damage at Hilo revealed much evidence of the tremendous forces developed by the waves. Twenty-ton boulders had been moved hundreds of feet, asphaltic concrete pavements were peeled from their subbase, and hundreds of automobiles were tossed around and crushed.[3]

Tsunami Inundation

8. Tsunami inundation is the flooding during part of a tsunami

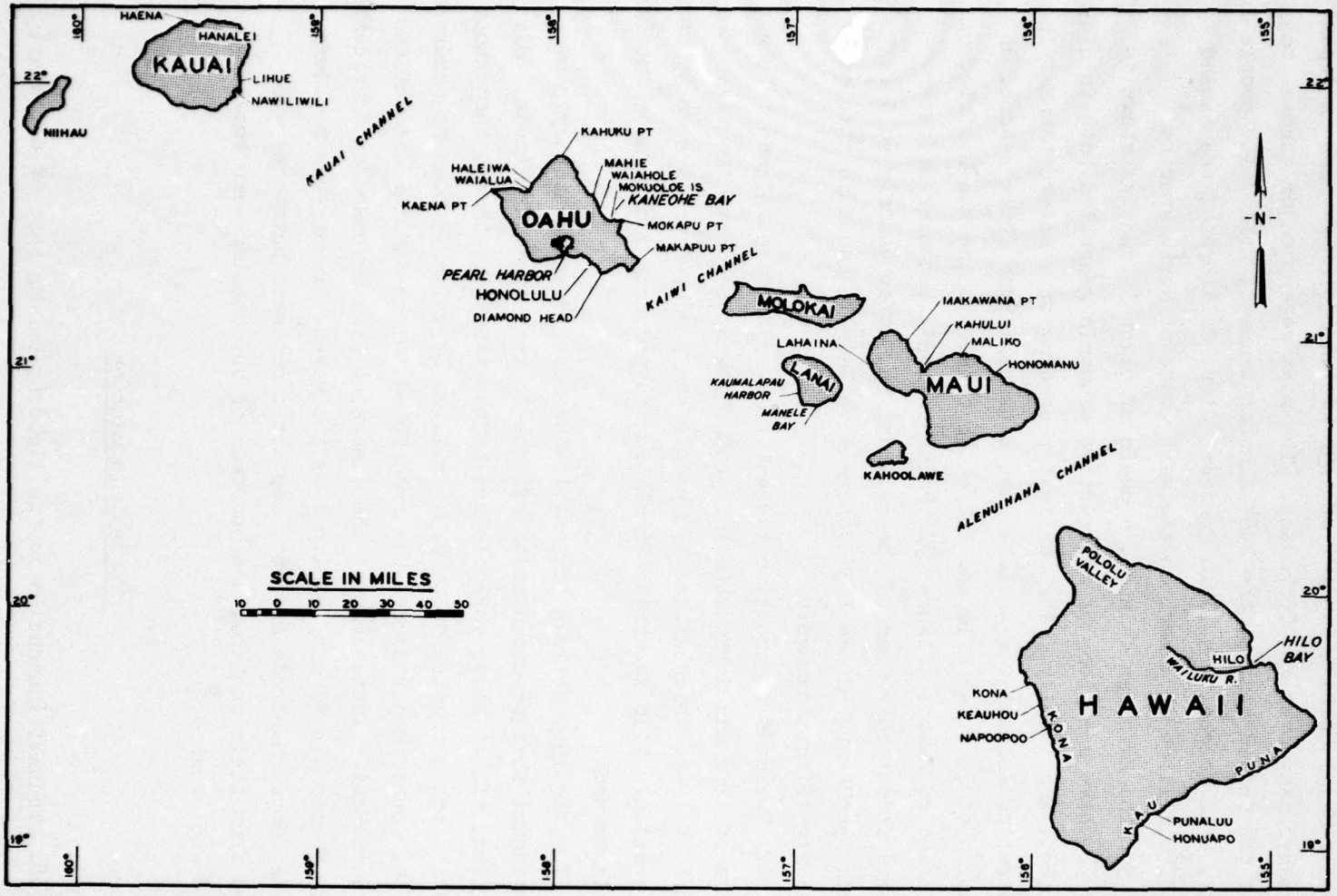

Figure 1. The Hawaiian Islands

event of land that is normally dry. Inundation is used in this report without any necessary implication of severe damage or great water depths. Dry land areas flooded during a tsunami are in the region of inundation.

9. Characteristics of tsunami inundation are not well known since there have been few surveys of both tsunami high-water marks near the shoreline and detailed measurements of inundation limits. Tsunamis in the Hawaiian Islands usually appear as rapidly rising water levels rather than bores. Thus runup should be similar to elevation at the shoreline, although runup may be greater or less than elevation at the shoreline due to flow divergence or convergence, time-dependence of the wave form, frictional effects, and topographic variations.

10. The similarity between runup and elevation at the shoreline is illustrated in the detailed surveys that have been performed. For example, Magoon[4] reports flooding to about the 20-ft contour above mean lower low water (mllw) and elevations at the shoreline of about 20 ft (mllw) for the 1964 tsunami at Crescent City, California. Wilson and Tørum[1] report that the 20-ft (mllw) runup at Valdez, Alaska, for the 1964 tsunami checks "well for consistency with water level measurements made on numerous buildings throughout the town." Similar comments were made by Brown[5] in reference to survey measurements of 30-ft (mllw) runup at Seward, Alaska, for the 1964 tsunami. Runup and elevation at the shoreline were similar at nine locations in Japan as recorded by Nasu[6] in surveys following the 1933 Sanriku tsunami. This tsunami had a short period (12 minutes) and reached an elevation as great as 28.7 metres at one survey location. Runup and elevation at the shoreline also were similar at Hilo, Hawaii, for the 1960 tsunami (borelike waves).[7] Differences are apparent, however, at locations where Eaton et al.[7] demonstrate that flow divergence is significant.

11. Tsunami inundation has been modeled using hydraulic models.[8,9] However, hydraulic models must be built large enough for scale effects not to be significant. Thus it is quite expensive to build hydraulic models for simulations of tsunamis. For example, although Hilo Harbor is small relative to the entire coastline of the

Hawaiian Islands, a hydraulic model of this harbor that was used for tsunami studies was required to be of moderate size (right triangular shape with sides measuring 63 and 93 ft) even with a small horizontal scale of 1:600 and a three to one distortion.[8]

12. There have been several analytical and numerical studies of one-dimensional tsunami runup.[10-13] Comparisons were not made in these studies of predicted runup and actual inundation during historical tsunamis. The one-dimensional nature of the solutions and also the borelike waves considered in the studies make these studies inappropriate for most practical applications. A recent study by Bretschneider and Wybro[14] employs a one-dimensional analytic solution to determine tsunami runup for both bores and nonbores. Frictional effects and linear ground slopes are included in the solution. Comparisons are presented of calculated and measured runup of actual historical tsunamis. The main drawbacks of this approach are the one-dimensional and time-independent properties of the solution.

13. A one-dimensional empirical method based upon trial-and-error comparisons of calculated (assuming various initial elevations and rates of elevation decay during propagation over land) and measured runup during historical tsunamis in Hawaii has been presented by Cox.[15] Cox sought criteria by which the long-term limits of potential inundation might be estimated with necessary safety margins. Prior to this work the Civil Defense of the State of Hawaii warned people to evacuate areas where the land elevation was less than 50 ft above sea level. In some areas such as Honolulu, such an evacuation area would have been much larger than could have been evacuated or would have needed to have been evacuated. Cox found that an assumed initial total energy head of 50 ft (at a location where the water depth was 10 ft below msl) and a one percent decline with distance traversed (1-ft decay for every 100 ft of travel) would provide an estimate of the potential inundation limits that appeared reasonable when compared with historical records. Somewhat different criteria were applied at certain other locations.

14. Two-dimensional numerical models have not been developed to simulate tsunami inundation. The pioneering work in numerical models

for flooding problems was a study of storm surges in Galveston Bay, Texas, by Reid and Bodine.[16] An extension of this work was performed by Masch et al.[17] and applied to tidal hydrodynamics problems.

Purpose of Study

15. The purpose of this study was to develop a method to determine two-dimensional and time-dependent tsunami (nonbore) inundation based upon a numerical model developed recently at the WES for numerical simulations of tidal hydrodynamics.[18] Such a method is needed by the U. S. Army Engineer Division, Pacific Ocean (POD), to delineate inundation limits of tsunamis based upon elevations near the shoreline predicted for the Hawaiian Islands in a previous WES report.[19] Inundation limits are required by POD for use in tsunami flood hazard evaluations for floodplain management and flood insurance rate calculations.

PART II: NUMERICAL MODEL

Equations of Motion

16. The hydrodynamic equations governing tsunami propagation in the nearshore region and inundation are derived from the classical Navier-Stokes equations expressed in a Cartesian coordinate system.[20] Since tsunamis have lengths much greater than the water depths over which they propagate, fluid motions are approximately two-dimensional. Thus vertical fluid velocities and accelerations are small in comparison with horizontal velocities and accelerations, respectively. If the fluid is assumed to be homogeneous and incompressible and the flow is integrated from the sea bottom to the free water surface, the usual long wave equations are obtained:

$$\frac{\partial U}{\partial t} + \frac{U}{d}\frac{\partial U}{\partial x} + \frac{V}{d}\frac{\partial U}{\partial y} + gd\frac{\partial \eta}{\partial x} + \frac{gU}{C^2 d^2}\left(U^2 + V^2\right)^{1/2} = 0 \qquad (1)$$

$$\frac{\partial V}{\partial t} + \frac{U}{d}\frac{\partial V}{\partial x} + \frac{V}{d}\frac{\partial V}{\partial y} + gd\frac{\partial \eta}{\partial y} + \frac{gV}{C^2 d^2}\left(U^2 + V^2\right)^{1/2} = 0 \qquad (2)$$

$$\frac{\partial \eta}{\partial t} + \frac{\partial U}{\partial x} + \frac{\partial V}{\partial y} = 0 \qquad (3)$$

where

U = vertically integrated transport per unit width in x direction*

t = time

$d = \eta - h$, total water depth

h = still-water depth

x,y = Cartesian coordinates

V = vertically integrated transport per unit width in y direction

---

* For convenience, symbols and unusual abbreviations are listed and defined in the Notation (Appendix A).

g = acceleration due to gravity

η = water-surface elevation

C = Chezy frictional coefficient

17. The terms $\frac{gU}{C^2d^2}(U^2 + V^2)^{1/2}$ and $\frac{gV}{C^2d^2}(U^2 + V^2)^{1/2}$ are bottom friction terms derived from experiments and theoretical considerations for one-dimensional flow in a river.[21] Previous efforts[22,23] in numerical modeling of long waves have shown that these terms adequately represent the damping of long waves due to the shear at the sea bottom.

18. The Chezy frictional coefficient is given by the expression

$$C = \frac{1.486}{n_m} d^{1/6} \tag{4}$$

where n_m is Manning's n. Manning's n is empirically determined and depends upon characteristics of the land over which water is flowing.

19. The advective terms in Equations 1 and 2 (second and third terms) are neglected in this study. These terms often cause difficulties in numerical modeling since they generate higher harmonics of waves and intensify vorticity through stretching of vortex lines. The generation of higher harmonics may create problems since the cascading of energy from longer to shorter waves will result in energy accumulation in waves with a wavelength of twice the grid spacing of the numerical grid. This accumulation may result in numerical instability. Difficulties in modeling the generation and dissipation of vorticity also can result in eddy formations that may produce numerical instability.

20. The advective terms are not important in determining the extent of tsunami inundation. These terms were found to have a negligible effect on the extent of tsunami inundation in tests (with and without advective terms) of the numerical model presented later in this report. Accurate numerical simulations of hurricane surge and tidal elevations have been made in the past, solving equations that neglect the advective terms.[24]

Variable Grid

21. Tsunami inundation is difficult to model since tsunamis have great wavelengths. Wavelengths even in shallow water are much greater than extents of inland flooding or length scales of bathymetric and topographic variations near the coastline. The input boundary of a numerical grid must be at least one-half a wavelength away from the coastline, since the form of the waves reflected from the coast is not known a priori at the input boundary. Thus the forcing function at the input boundary cannot be varied to account for both the incident and reflected wave. This makes it necessary to move the input boundary far enough away from the coast that waves are not reflected at this boundary.

22. The numerical model[18] employed in this study uses a smoothly varying grid that allows cells to be small in the inundation region and large in the ocean. A piecewise reversible transformation (analogous to that used in Reference 25) is used independently in the x- and y-directions to map the variable grid into a uniform grid used in the computational space. The transformation has the form

$$x = a_1 + b_1 \alpha_1^{c_1} \tag{5}$$

$$y = a_2 + b_2 \alpha_2^{c_2} \tag{6}$$

where $a_1, b_1, c_1, a_2, b_2, c_2$ are arbitrary constants and α_1 and α_2 are coordinates in the computational space. This transformation allows all derivatives to be centered in the computational space. Many stability problems commonly occurring in variable grid schemes are eliminated using this transformation since the real space grid is smoothly varying with the variation and its first derivative being continuous.

23. The equations of motion (Equations 1-3) have the following form in the computational space:

$$\frac{\partial U}{\partial t} + \frac{gd}{\mu_1}\frac{\partial \eta}{\partial \alpha_1} + \frac{gU}{C^2 d^2}\left(U^2 + V^2\right)^{1/2} = 0 \qquad (7)$$

$$\frac{\partial V}{\partial t} + \frac{gd}{\mu_2}\frac{\partial \eta}{\partial \alpha_2} + \frac{gV}{C^2 d^2}\left(U^2 + V^2\right)^{1/2} = 0 \qquad (8)$$

$$\frac{\partial \eta}{\partial t} + \frac{1}{\mu_1}\frac{\partial U}{\partial \alpha_1} + \frac{1}{\mu_2}\frac{\partial V}{\partial \alpha_2} = 0 \qquad (9)$$

where

$$\mu_1 = \frac{\partial x}{\partial \alpha_1} = b_1 c_1 \alpha_1^{\,c_1 - 1} \qquad (10)$$

$$\mu_2 = \frac{\partial y}{\partial \alpha_2} = b_2 c_2 \alpha_2^{\,c_2 - 1} \qquad (11)$$

The variables μ_1 and μ_2 define the stretching of the uniform computational grid to form the variable spaced grid in real space.

Computational Techniques

24. The numerical model[18] uses a space-staggered scheme in which flows and water levels are defined at different locations in the grid (Figure 2) to form the finite difference approximations of Equations 7-9. A multioperational alternating-direction technique developed by Leendertse[22] is used in the solution algorithm. Computations are separated into two cycles corresponding to a sweep of the grid in the α_1 and α_2 directions. The first cycle computes η and U implicitly, advancing the time from $k\Delta t$ to $(k + 1/2)\Delta t$. A system of linear algebraic equations whose coefficient matrix is tridiagonal is produced by applying a centered difference operator to Equations 7 and 9 along a grid line parallel to the x-axis. The difference expressions for Equations 7 and 9 for the first cycle are given by the following equations:

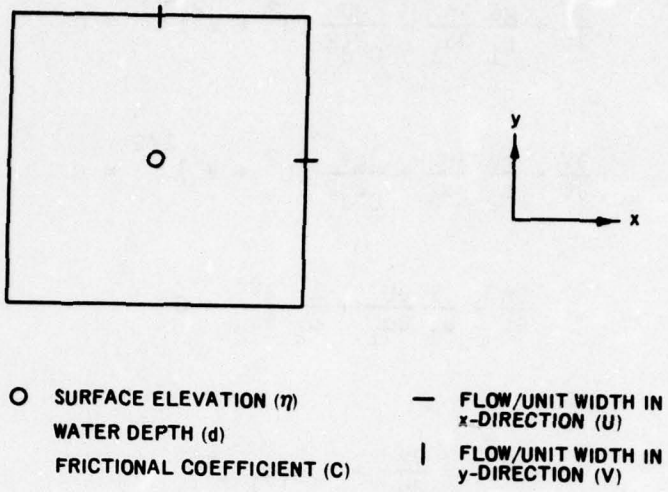

Figure 2. Space-staggered scheme

$$U^{k+1/2}_{n,m+1/2} = U^{k-1/2}_{n,m+1/2} + \Delta t\left(-\frac{g}{2\Delta\alpha_1}\left(\frac{d^*}{\mu_1}\right)_{n,m+1/2}\left\{\eta^{k+1}_{n,m+1} - \eta^{k+1/2}_{n,m} + \eta^{k-1/2}_{n,m+1} - \eta^{k-1/2}_{n,m}\right\}\right.$$

$$\left. - \frac{g\left(U^{k+1/2}_{n,m+1/2} + U^{k-1/2}_{n,m+1/2}\right)}{\left(2\, d^*\bar{\bar{C}}^k\right)^2}\left[\left(U^{k-1/2}_{n,m+1/2}\right)^2 + \bar{\bar{V}}^2_{n,m+1/2}\right]^{1/2}\right) \quad (12)$$

$$\eta^{k+1/2}_{n,m} = \eta^{k}_{n,m} - \frac{\Delta t}{2}\left[\frac{1}{\Delta\alpha_1\left(\mu_1\right)_m}\left(U^{k+1/2}_{n,m+1/2} - U^{k+1/2}_{n,m-1/2}\right)\right.$$

$$\left. + \frac{1}{\Delta\alpha_2\left(\mu_2\right)_n}\left(V^{k}_{n+1/2,m} - V^{k}_{n-1/2,m}\right)\right] \quad (13)$$

where $d^* = \bar{\eta}^k - \bar{h}$ and Δt is the time-step for completing two cycles. A single bar over a variable represents a two-point average and a double bar a four-point average. The subscripts m and n correspond to

spatial locations and the superscript k to time levels. If terms are collected that are to be computed along line n at time level $(k + 1/2)\Delta t$, Equations 12 and 13 can be expressed as follows:

$$-a_m \eta^{k+1/2}_{n,m} + \bar{a}_{m+1/2} U^{k+1/2}_{n,m+1/2} + a_{m+1} \eta^{k+1/2}_{n,m+1} = B_{m+1/2} \tag{14}$$

$$-a_{m-1/2} U^{k+1/2}_{n,m-1/2} + \eta^{k+1/2}_{n,m} + a_{m+1/2} U^{k+1/2}_{n,m+1/2} = A_m \tag{15}$$

where

$$A_m = \eta^k_{n,m} - \frac{\Delta t}{2(\mu_2)_n \Delta\alpha_2} \left(V^k_{n+1/2,m} - V^k_{n-1/2,m} \right) \tag{16}$$

$$B_{m+1/2} = U^{k-1/2}_{n,m+1/2} + \Delta t \left(- \frac{gd^*}{2(\mu_1)_m \Delta\alpha_1} \left\{ \eta^{k-1/2}_{n,m+1} - \eta^{k-1/2}_{n,m} \right\} \right.$$

$$\left. - \frac{g\, U^{k-1/2}_{n,m+1/2}}{2\bar{C}^2 (d^*)^2} \left[\left(U^{k-1/2}_{n,m+1/2} \right)^2 + \bar{\bar{V}}^2 \right]^{1/2} \right) \tag{17}$$

The coefficients are defined as follows:

$$a_{m-1/2} = a_{m+1/2} = \frac{\Delta t}{2(\mu_1)_m \Delta\alpha_1} \tag{18}$$

$$a_m = a_{m+1} = \frac{g\Delta t d^*}{2(\mu_1)_m \Delta\alpha_1} \tag{19}$$

$$\bar{a}_{m+1/2} = 1 + \frac{g\Delta t}{2\bar{C}^2(d^*)^2}\left[\left(U^{k-1/2}_{n,m+1/2}\right)^2 + \bar{\bar{V}}^2\right]^{1/2} \tag{20}$$

25. Assuming that $\eta_M^{k+1/2}$ is a given water level at the lower boundary and $U_{L+1/2}^{k+1/2}$ is a given flow at the upper boundary, the matrix form of the equations for line n can be written as follows:

$$\begin{bmatrix} \bar{a}_{M+1/2} & a_{M+1} & 0 & 0 & \cdots & 0 \\ -a_{M+1/2} & 1 & a_{M+3/2} & 0 & \cdots & 0 \\ 0 & -a_{M+1} & \bar{a}_{M+3/2} & a_{M+2} & \cdots & 0 \\ & & & \cdots & & \\ & & & \cdots & & \\ & & & \cdots & & \\ 0 & 0 & 0 & \cdots & -a_{L-1/2} & 1 \end{bmatrix} \begin{bmatrix} U_{M+1/2} \\ \eta_{M+1} \\ U_{M+3/2} \\ \cdot \\ \cdot \\ \cdot \\ \eta_L \end{bmatrix}^{k+1/2} = \begin{bmatrix} \hat{B}_{M+1/2} \\ A_{M+1} \\ B_{M+3/2} \\ \cdot \\ \cdot \\ \cdot \\ \hat{A}_L \end{bmatrix}^k \tag{21}$$

26. The above system of equations is tridiagonal and can be solved with a minimum number of operations by performing the process of elimination using a set of recursive formulas. Equation 14 is expressed as follows:

$$U^{k+1/2}_{m+1/2} = - R_m \eta^{k+1/2}_{m+1} + S_m \tag{22}$$

where

$$R_m = \frac{a_{m+1}}{\bar{a}_{m+1/2}}; \quad S_m = \frac{\hat{B}_{m+1/2}}{\bar{a}_{m+1/2}} \tag{23}$$

and

$$\hat{B}_{m+1/2} = B_{m+1/2} + a_m \eta_M^{k+1/2} \tag{24}$$

Substitution of Equation 21 into the Equation 15 yields

$$-a_{m+1/2}\left(-R_m \eta_{m+1}^{k+1/2} + S_m\right) + \eta_{m+1}^{k+1/2} + a_{m+3/2} U_{m+3/2}^{k+1/2} = A_{m+1} \tag{25}$$

or

$$\eta_{m+1}^{k+1/2} = -P_{m+1} U_{m+3/2}^{k+1/2} + Q_{m+1} \tag{26}$$

where

$$P_{m+1} = \frac{a_{m+3/2}}{1 + a_{m+1/2} R_m} \tag{27}$$

$$Q_{m+1} = \frac{A_{m+1} + a_{m+1/2} S_m}{1 + a_{m+1/2} R_m} \tag{28}$$

Again, the flow rate can be expressed as a function of the next water level using Equation 14.

$$U_{m+3/2}^{k+1/2} = -R_{m+1} \eta_{m+2} + S_{m+1} \tag{29}$$

where

$$R_{m+1} = \frac{a_{m+2}}{\bar{a}_{m+3/2} + a_{m+1} R_{m+1}} \tag{30}$$

$$S_{m+1} = \frac{B_{m+3/2} + a_{m+1} Q_{m+1}}{\bar{a}_{m+3/2} + a_{m+1} R_{m+1}} \tag{31}$$

In general, the recursion formulas can be written as follows:

$$\eta_m^{k+1/2} = -P_m \, U_{m+1/2}^{k+1/2} + Q_m \tag{32}$$

where

$$U_{m-1/2}^{k+1/2} = -R_{m-1} \, S_m^{k+1/2} + S_{m-1} \tag{33}$$

where

$$T1 = 1 + a_{m-1/2} \, R_{m-1} \qquad T2 = \bar{a}_{m+1/2} + a_m \, P_m$$

$$P_m = \frac{a_{m+1/2}}{T1} \qquad Q_m = \frac{A_m + a_{m-1/2} \, S_{m-1}}{T1} \tag{34}$$

$$R_m = \frac{a_{m+1}}{T2} \qquad S_m = \frac{B_{m+1/2} + a_m \, Q_m}{T2}$$

27. Fractional subscripts are not permitted in the FORTRAN computer code. Therefore, in the computer code a different index system is adopted. Water levels, depths, frictional coefficients, and flows appearing in the cell shown in Figure 2 have the same coordinate index (N,M) . Using this notation, the coefficients given in Equations 26, 27, and 29-30 are expressed as follows:

$$P_M = \frac{\tau}{(\mu_1)_{2M-1} \Delta\alpha_1} \Bigg/ \left[1 + \frac{\tau}{(\mu_1)_{2M-1} \Delta\alpha_1} R_{M-1} \right] \tag{35}$$

$$Q_M = \left[A_M + \frac{\tau}{(\mu_1)_{2M-1} \Delta\alpha_1} S_{M-1} \right] \Bigg/ \left[1 + \frac{\tau}{(\mu_1)_{2M-1} \Delta\alpha_1} R_{M-1} \right] \tag{36}$$

$$R_M = \frac{gd^* \tau}{(\mu_1)_{2M} \Delta\alpha_1} \Bigg/ D1 \tag{37}$$

$$S_M = \left[B_M + \frac{g\tau}{\left(\mu_1\right)_{2M} \Delta\alpha_1} d^* Q_M \right] \Big/ D1 \tag{38}$$

where

$$D1 = 1 + \frac{4g\tau}{\left[d^*\left(C_{N,M+1} + C_{N,M}\right)\right]^2} \cdot \left[\left(U^{k-1/2}_{N,M} \right)^2 + \bar{\bar{V}}^2 \right]^{1/2}$$

$$+ \frac{g\tau}{\left(\mu_1\right)_{2M} \Delta\alpha_1} d^* P_M \tag{39}$$

$$A_M = \eta^k_{N,M} - \frac{\tau}{\left(\mu_2\right)_{2N-1} \Delta\alpha_2} \left(V^k_{N,M} - V^k_{N-1,M} \right) + \tau \hat{R}^k_{N,M} \tag{40}$$

$$B_M = U^{k-1/2}_{N,M} + \tau \left(- \frac{gd^*}{\left(\mu_1\right)_{2M} \Delta\alpha_1} \left\{ \eta^{k-1/2}_{N,M+1} - \eta^{k-1/2}_{N,M} \right\} \right.$$

$$\left. - \frac{4g\, U^{k-1/2}_{N,M}}{\left[d^*\left(C_{N,M} + C_{N,M+1}\right)\right]^2} \left[\left(U^{k-1/2}_{N,M} \right)^2 + \bar{\bar{V}}^2 \right]^{1/2} \right) \tag{41}$$

$$d^* = 1/2 \left(\eta^k_{N,M+1} + \eta^k_{N,M} - h_{N,M+1} - h_{N,M} \right) \tag{42}$$

$$\bar{\bar{V}} = 1/4 \left(V^k_{N-1,M} + V^k_{N,M} + V^k_{N-1,M+1} + V^k_{N,M+1} \right) \tag{43}$$

$$\tau = \frac{\Delta t}{2} \tag{44}$$

28. The solution Equations 21 and 31 can be expressed as follows:

$$U^{k+1/2}_{N,M-1} = -R_{M-1}\, \eta^{k+1/2}_{N,M} + S_{M-1} \tag{45}$$

$$\eta^{k+1/2}_{N,M} = -P_M\, U^{k+1/2}_{N,M} + Q_M \tag{46}$$

29. The recursion coefficients of Equations 34-37 can be computed in succession between boundaries on line N. Various approximations of these coefficients are required depending upon the types of boundary conditions that are applied. The solution Equations 45 and 46 can be solved for all surface elevations and flows in descending order once the set of coefficients has been calculated.

30. The second cycle computes η and V implicitly, advancing the time from $(k + 1/2)\Delta t$ to $(k + 1)\Delta t$. The recursion formulas for this cycle are very similar to those given for the first cycle. These formulas for the second cycle (applied along a line m) can be expressed as follows:

$$V^{k+1}_{n+1/2,m} = V^{k}_{n+1/2,m} + \Delta t \left(- \frac{g}{2\Delta\alpha_2} \left(\frac{\hat{d}}{\mu_2} \right)_{n+1/2,m} \left\{ \eta^{k+1}_{n+1,m} \right.\right.$$

$$\left. - \eta^{k+1}_{n,m} + \eta^{k}_{n+1,m} - \eta^{k}_{n,m} \right\} + \frac{g\left(V^{k+1}_{n+1/2,m} + V^{k}_{n+1/2,m} \right)}{\left(2\, \hat{a}\, \bar{C}^{k} \right)^2}$$

$$\left. \cdot \left[\bar{\bar{U}}^{2}_{n+1/2,m} + \left(V^{k}_{n+1/2,m} \right)^2 \right]^{1/2} \right) \tag{47}$$

$$\eta_{n,m}^{k+1} = \eta_{n,m}^{k+1/2} - \frac{\Delta t}{2}\left[\frac{1}{\Delta\alpha_1\left(\mu_1\right)_m}\left(U_{n,m+1/2}^{k+1/2} - U_{n,m-1/2}^{k+1/2}\right)\right.$$

$$\left. + \frac{1}{\Delta\alpha_2\left(\mu_2\right)_n}\left(V_{n+1/2,m}^{k+1} - V_{n-1/2,m}^{k+1}\right)\right] \tag{48}$$

where

$$\hat{d} = \bar{\eta}^{k+1/2} - \bar{h}$$

31. The recursion formulas for the second cycle can be written in the same notation as Equations 34-46.

$$P_N = \frac{\tau}{\left(\mu_2\right)_{2N-1}\Delta\alpha_2} \Bigg/ \left[1 + \frac{\tau}{\left(\mu_2\right)_{2N-1}\Delta\alpha_2} R_{N-1}\right] \tag{49}$$

$$Q_N = \left[A_N + \frac{\tau}{\left(\mu_2\right)_{2N-1}\Delta\alpha_2}\right] \Bigg/ \left[1 + \frac{\tau}{\left(\mu_2\right)_{2N-1}\Delta\alpha_2} R_{N-1}\right] \tag{50}$$

$$R_N = \frac{g\tau\hat{d}}{\left(\mu_2\right)_{2N}\Delta\alpha_2} \Bigg/ D2 \tag{51}$$

$$S_N = \left[B_N + \frac{g\tau\hat{d}}{\left(\mu_2\right)_{2N}\Delta\alpha_2} Q_N\right] \Bigg/ D2 \tag{52}$$

where

$$D2 = 1 + \frac{4g\tau}{\left[\hat{d}\left(C_{N+1,M} + C_{N,M}\right)\right]^2} \cdot \left[\bar{\bar{U}}^2 + \left(V_{N,M}^{k}\right)^2\right]^{1/2} + \frac{g\tau\hat{d}}{\left(\mu_2\right)_{2N}\Delta\alpha_2} P_N \tag{53}$$

$$A_N = \eta_{N,M}^{k+1/2} - \frac{\tau}{\left(\mu_1\right)_{2M-1}\Delta\alpha_1}\left(U_{N,M}^{k+1/2} - U_{N,M-1}^{k+1/2}\right) + \tau\,\hat{R}_{N,M}^{k+1/2} \tag{54}$$

$$B_N = V^k_{N,M} - \tau \left(+ \frac{g\hat{d}}{\left(\mu_2\right)_{2N} \Delta\alpha_2} \left\{ \eta^k_{N+1,M} - \eta^k_{N,M} \right\} + \frac{4g\, V^k_{N,M}}{\left[\hat{d}\left(C_{N+1,M} + C_{N,M}\right)\right]^2} \left[\bar{\bar{U}}^2 + \left(V^k_{N,M}\right)^2 \right]^{1/2} \right) \tag{55}$$

$$\hat{d} = 1/2\left(\eta^{k+1/2}_{N+1,M} + \eta^{k+1/2}_{N,M} - h_{N+1,M} - h_{N,M}\right) \tag{56}$$

$$\bar{\bar{U}} = 1/4\left(U^{k+1/2}_{N+1,M} + U^{k+1/2}_{N+1,M-1} + U^{k+1/2}_{N,M-1} + U^{k+1/2}_{N,M}\right) \tag{57}$$

32. The solution Equations 21 and 31 can be expressed as follows:

$$\eta^{k+1}_{N,M} = -P_N\, V^{k+1}_{N,M} + Q_N \tag{58}$$

$$V^{k+1}_{N-1,M} = -R_{N-1}\, \eta^{k+1}_{N,M} + S_{N-1} \tag{59}$$

Boundary Conditions

33. There are four types of boundaries used in the numerical model. The first is a seaward boundary that terminates the computational grid. Water levels are prescribed as a function of location and time at this boundary. Thus, water levels may vary along the input boundary. Water level time-histories can either be arbitrary with elevations supplied in tabular form or sinusoidal with the amplitude and period prescribed.

34. A second boundary used is located at the land-water interface. The no-flow condition normal to this boundary is the usual boundary condition employed in the numerical computations. Thus $U = 0$ or $V = 0$

is prescribed at the appropriate grid cell face. The model also handles the flooding and drying of land. Inundation is simulated by making the location of land-water boundary a function of local water elevations. The possibility of inundation is established by continual monitoring of water levels in adjacent grid cells. Initial movement of water onto previously dry grid cells is controlled by a broad-crested weir formula.[16] Once the water level on a previously dry cell exceeds some small prescribed value, the boundary face is treated as being open and computations for η, U, and V are the same as for any ocean cell. The drying of cells follows the inverse process.

35. Exposed, submerged, and overtopping barriers defined along grid cell faces form a third type of boundary. Exposed barriers have no-flow conditions prescribed across appropriate grid cell faces. Flow across a submerged barrier is controlled by use of a time-dependent frictional coefficient. Overtopping barriers are barriers that are exposed (with no-flow conditions) during times of a simulation and submerged at other times. The overtopping of a barrier is controlled by using a broad-crested weir formula to specify proper flow rates across the barrier. Water is transferred from the high to low side using this formula. Once the barrier is submerged (or exposed) the procedures used for submerged (or exposed) barriers are applied.

36. A no-flow condition normal to the boundary is used for the lateral ocean boundaries of the computational grid. The waves reflected from the shoreline have only small propagation vector components in a direction perpendicular to these boundaries. There is some reflection from these boundaries; however, the reflected waves still move away from the shoreline until they reach the input boundary. Computations are stopped before reflections from these lateral boundaries are a problem. The lateral boundaries may introduce small errors in the immediate vicinity of the intersection of these boundaries with the land-water interface.

PART III: VERIFICATION

Introduction

37. There have been few extensive surveys of tsunami high-water marks near the shoreline and detailed measurements of inundation levels in addition to recordings of tsunami wave forms. The only two tsunamis in the United States for which such data are available are the 1960 Chilean tsunami recorded at Hilo, Hawaii, and the 1964 Alaskan tsunami recorded at Crescent City, California. However, the incident wave form for the 1960 tsunami at Hilo was quite complex. The major waves of this tsunami at Hilo were bores. Wiegel[26] indicates that Mach reflection of a wave may have occurred on the cliffs of the west side of Hilo Bay with the Mach-stem wave moving toward the Hilo area. This Mach-stem wave may have superposed on the diffracted incident wave at Hilo.[8] Tsunami elevations recorded near the shoreline for this tsunami vary quite rapidly along the shoreline. The 1960 tsunami at Hilo was not used for verification purposes in this study, since the incident waves for this tsunami were bores; the complex Mach-stem effect may have developed; and waves traveling in different directions may have superposed with unknown phases. The lack of knowledge concerning the incident and reflected waves would make simulations of this tsunami difficult even if the model could handle bores.

38. The 1964 tsunami at Crescent City, California (Figure 3), was used to verify the numerical model discussed in PART II. The simulation of this tsunami is an excellent verification test since the tsunami was quite large at Crescent City and the region has many complex features. For example, the Crescent City Harbor is protected by breakwaters, some of which were overtopped and others which were not. In the region there is a developed city area, mud flats, and an extensive riverine floodplain. Inland flooding was extensive in the floodplain area and extended as much as a mile inland. Sand dunes and elevated roads played a prominent role in limiting flooding in certain areas. Verification of the model for this complex region makes the model quite

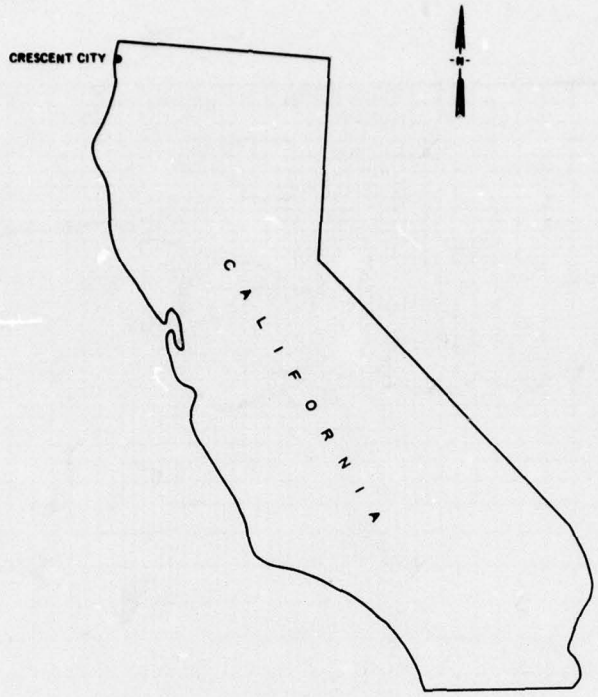

Figure 3. Location map for Crescent City, California

general so that it can be applied to any region.

39. Magoon[4] reports surveys of the Crescent City region made by the Corps of Engineers following the 1964 tsunami. The maximum limits of inundation and high-water marks were recorded in the surveys. Wiegel[27] presents characteristics of the wave form and details of the interaction of the tsunami with the Crescent City region.

Numerical Grid and Boundary Conditions

40. Figure 4 shows the numerical grid used in the simulation of the 1964 tsunami at Crescent City. Grid cells are concentrated in the Crescent City and Crescent City Harbor area. The grid is oriented such that the incident wave approaches Crescent City from the direction predicted by refraction diagrams for this tsunami presented by Roberts and Kauper.[28] The ocean bathymetry is reproduced out to the 30-ft contour

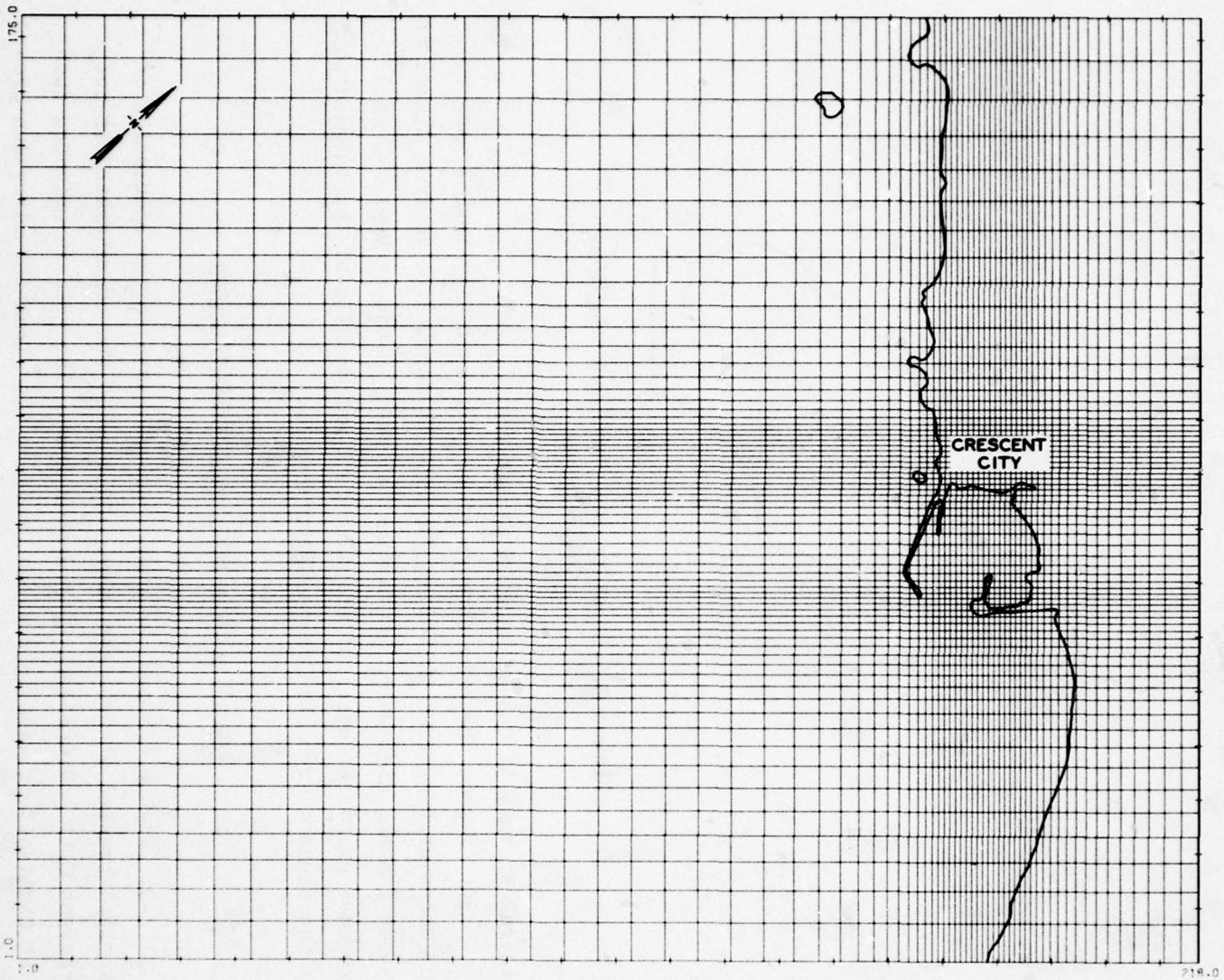

Figure 4. Numerical grid for Crescent City region

(mllw). Beyond this contour, the ocean is a constant 30-ft depth (mllw). This constant depth region allows the input boundary to be moved sufficiently distant (at least one-half the total wave form of interest) from the shoreline that waves do not reflect from the input boundary. The variable nature of the grid allows the input boundary to be placed far from the region of interest without creating so many grid cells that computational time becomes excessive. A uniform grid with cells the size of the smallest cells in Figure 4 would require a computational time of approximately 25 times greater than that required for the variable grid shown in Figure 4.

41. The input to the numerical model is a wave crest that, when propagated to shore, reproduces as accurately as possible the historical maximum elevation at the tide-gage location near the shoreline in Crescent City Harbor. The tide gage was destroyed during the 1964 tsunami; however, Wilson and Tørum[1] inferred the form of the wave from the tide gage recording prior to destruction in addition to other evidence. There is some disagreement among investigators as to the maximum elevation of the tsunami at the tide gage. Estimates range from 18 to 20.7 ft above mllw. However, according to Wiegel,[27] the 20.7-ft elevation was recorded on land at a distance of approximately 1000 ft from the tide gage and it included a 1- to 2-ft contribution from local runup on a concrete wall. An earlier study by Keulegan et al.[29] considered all available information and concluded that the maximum elevation at the tide gage was 19 ft above mllw. A wave crest with an elevation of 19 ft above mllw at the tide-gage location was used in the numerical simulation.

42. There are several barriers in the Crescent City region. Wiegel[27] reports that there was little flow over the outer breakwater (Figure 5). Therefore, this breakwater was represented as a non-overtopping barrier. However, the breakwaters attached to Whaler Island (Figure 5) were overtopped during a part of the tsunami and thus are represented as dynamic overtopping barriers. Similarly, Redwood Highway (Figure 5) and beach dunes along the crest were overtopped during the 1964 tsunami. Water flowed over these barriers in a manner similar to

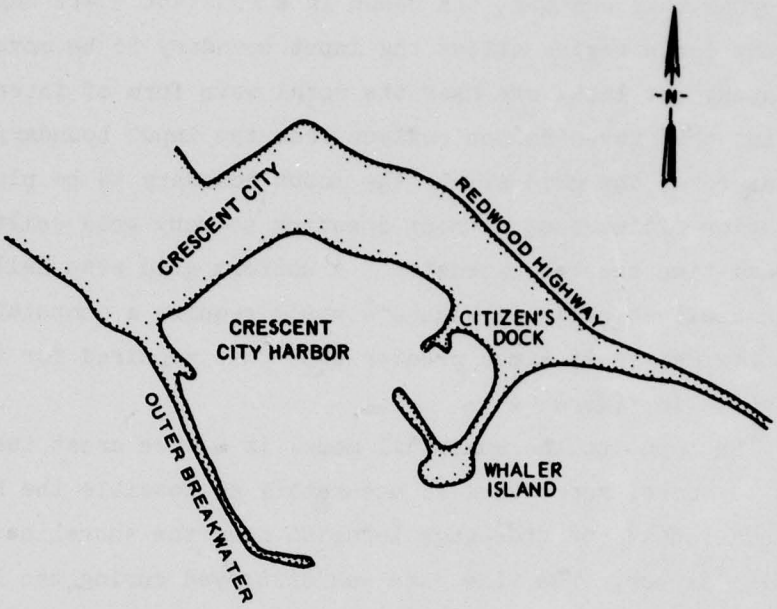

Figure 5. Crescent City Harbor area

water flowing over a broad weir and the runup was reduced.[4] These barriers also are represented as dynamic overtopping barriers with flow rates governed by weir equations.

43. Frictional effects in the numerical model are governed by the Chezy frictional coefficient given in Equation 4. A spatially varying Manning's n must be selected at the center of each grid cell shown in Figure 4. Manning's n is a function of the roughness of the ground and the vegetation. Values of Manning's n can be found in numerous references.[30,31] In this study, values of Manning's n suggested by Bretschneider and Wybro[14] for various coastal terrain conditions were used. Manning's n values were selected for very general categories of terrain, since detailed knowledge of vegetation and land roughness are usually not known for an area. For the Crescent City region, the ocean bottom, mud flats, and beaches were assigned a Manning's n equal to 0.024. Developed areas were assigned a value of 0.035 and the riverine floodplain area and other heavily vegetated areas a value of 0.055. No

attempt was made to force agreement of numerical calculations and historical recordings of elevations by varying local values of Manning's n.

44. Ocean depths and land elevations were taken from the Sister Rocks, California, quadrangle map published by the U. S. Geological Survey. Elevations in the city of Crescent City were taken from the detailed surveys of the Corps of Engineers as reported by Magoon.[4] Land elevations are not known accurately in the large floodplain area (Elk Creek) near Crescent City so elevations had to be estimated in this area.

Results

45. The Corps of Engineers made surveys of the tsunami inundation at Crescent City in January, April, and May of 1965 as reported by Magoon.[4] Figure 6 shows the location of 11 high-water marks recorded by the surveys. The tide gage was located at the end of Citizen's Dock

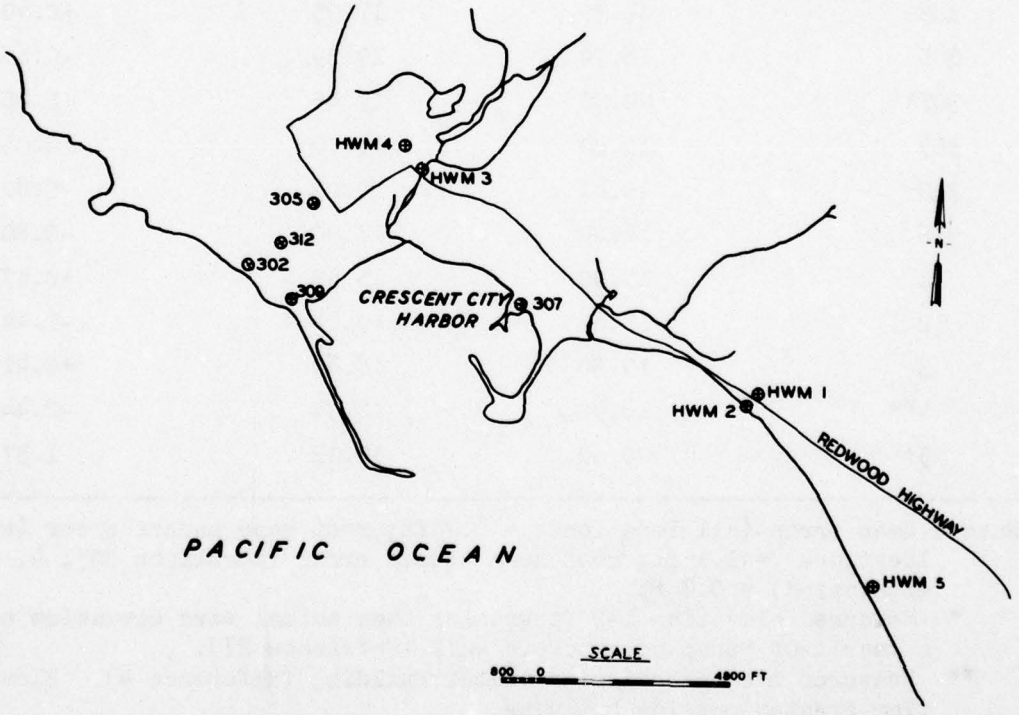

Figure 6. High-water mark locations for 1964 tsunami (adapted from Magoon, 1965)

(Figure 5) near high-water mark number 307. The following tabulation presents the measured elevations at the high-water marks and elevations calculated by the numerical model. The measured and calculated elevations are within 1 ft except at locations 307, 2, 3, and 5. However, Wiegel[27] reports that the measured elevation at location 307 was greater than the actual wave elevation by 1 to 2 ft due to local runup on a concrete wall. Thus the actual wave elevation and the calculated elevation are in good agreement at location 307. The measured elevation at location 4 is lower than the calculated elevation since the measured high-water mark was inside a lumber building. Incomplete filling of the lumber building by water would result in lower elevations within the building than those outside the building. Location number 5 is located

High-Water Mark Number (Reference 4)	Measured Elevation mllw, ft	Calculated Elevation mllw, ft	Difference ft
302	18.35	17.95	+0.40
305	18.74	19.39	-0.65
307*	20.70	19.45	+1.25
309	19.84	19.79	+0.05
312	19.41	20.23	-0.82
316	16.29	17.09	-0.80
1	15.90	15.43	+0.47
2	17.80	19.24	-1.44
3	19.30	18.89	+0.41
4**	16.50	18.94	-2.44
5†	20.50	19.13	1.37

Note: Mean error (all locations) = 0.2 ft; root mean square error (all locations) = 1.1 ft; root mean square error (locations 307, 4, 5 eliminated) = 0.7 ft.

* Measured elevation 1-2 ft greater than actual wave elevation as a result of runup on concrete wall (Reference 27).

** Measured elevation inside lumber building (Reference 4). Elevation greater outside building.

† Coastal location almost 2 miles south of tide gage. Incident wave amplitude likely to be somewhat different here than at tide gage location.

almost 2 miles south of the tide gage. It is likely that the wave approaching this shoreline had a greater elevation than the wave approaching the harbor area. The elevation calculated at this location could be increased by varying the incident wave form along the input boundary. There is no apparent explanation for the disagreement at location 2, especially since there is good agreement at nearby location 1.

46. The agreement between the measured high-water marks and calculated elevations is quite good. The root-mean-square error is 0.7 ft (elevations at locations 307, 4, and 5 not included since differences attributable to factors other than the numerical model). Since the observed elevation at the tide gage used to choose an incident wave height is accurate to within no more than 0.5 to 1 ft, the agreement between measured and calculated elevations is good.

47. Figure 7 shows contour lines of the tsunami elevation above ground level within the developed area of Crescent City. The topography and tsunami elevations are known in much more detail in this developed

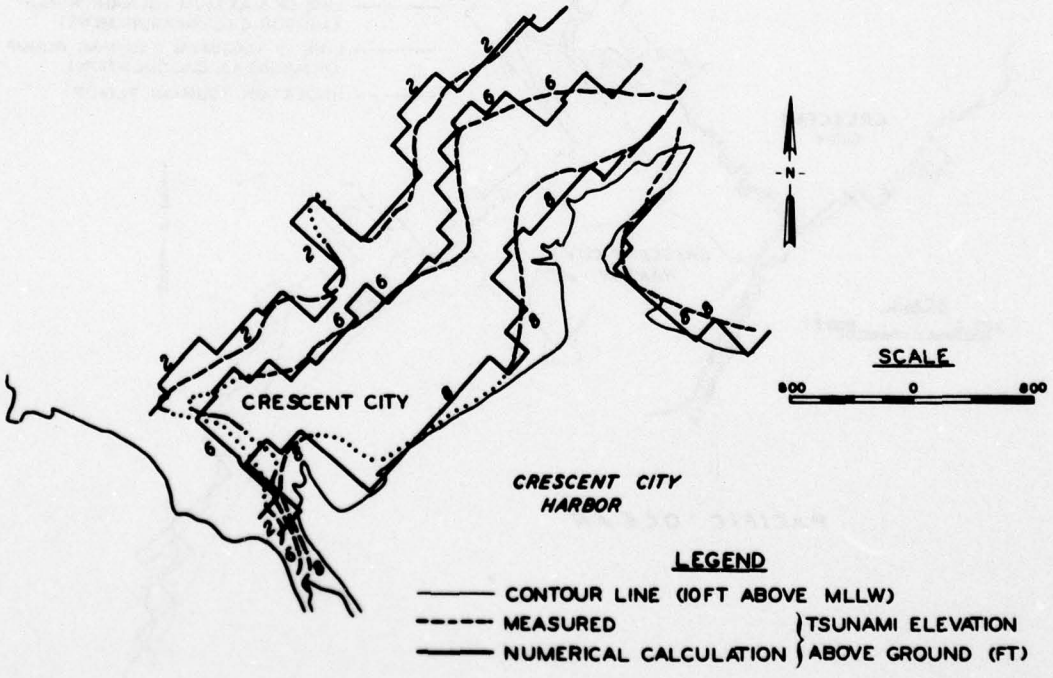

Figure 7. Inundation lines, 1964 tsunami (adapted from Magoon, 1965)

area than any other area. The dotted parts of the measured elevation dashed lines denote uncertain elevations. The contour lines for the calculated elevations were determined by linear interpolation. For example, if the elevation at the center of one cell was 9 ft above land and the elevation in an adjacent cell was 7 ft, the contour line was drawn half way between the two cell centers. The agreement between the measured and calculated elevations shown in Figure 7 is good.

48. Figure 8 shows inundation contours for the complete region surveyed by the Corps of Engineers. The most accurate contours are in the developed region of Crescent City. Contours in floodplain areas are of unknown accuracy, since the surveys were performed approximately one year after the tsunami. It may have been difficult to accurately determine inundation limits in the floodplain areas since there were no structures in these areas, debris lines may have been obliterated or difficult to differentiate from river-swept debris, and vegetation may

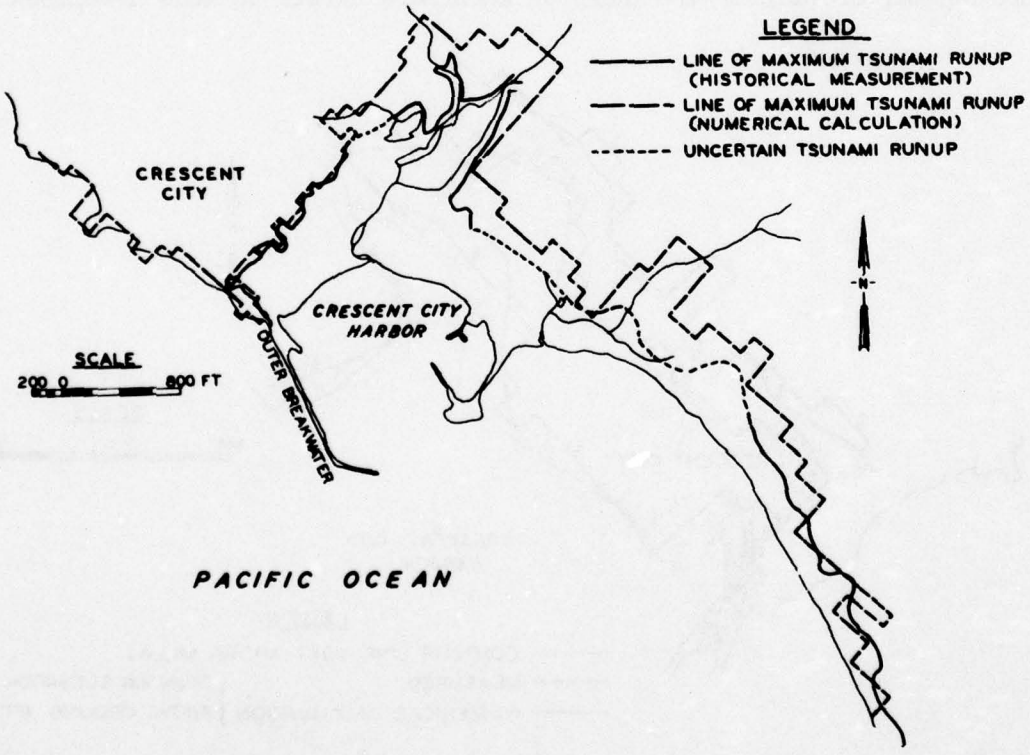

Figure 8. Flooding for 1964 tsunami (adopted from Magoon, 1965)

have recovered from salt damage as a result of the freshwater flow of the river system (winter rains occurred between the time of the tsunami and the surveys).

49. The measured and calculated inundation lines in the city area (Figure 8) are in excellent agreement. The calculated inundation lines are farther inland than the measured lines in the floodplain areas. In addition to the question of the accuracy of the measured inundation in the floodplain areas, the topography of the floodplains is not known accurately. The elevations of the floodplains are only known to be greater than mean sea level (msl) and less than 10 ft above msl. Elevations throughout this area had to be estimated in the topographic input to the numerical model. Elevations calculated at the extent of flooding in these floodplain areas were small (often a fraction of a foot). Land elevations could have been increased by small increments to have prevented flooding beyond the measured limits and thus forced agreement between measured and calculated limits. However, this was not done, since the accuracy of the survey measurements in these areas was questionable and the topography of floodplain areas is rarely accurate. Neither friction coefficients nor land elevations were varied in this verification to force agreement with measured elevations, since in an application of the numerical model to an arbitrary location these parameters would not be accurately known. The good agreements shown in Figure 7 and the tabulation on page 30 indicate that small inundation levels in distant floodplain areas do not have significant influence on elevations in other areas.

PART IV: APPLICATION TO HAUULA-PUNALUU, HAWAII

Introduction

50. The tsunami inundation numerical model was developed to allow the POD to determine inundation limits when tsunami elevations near the shoreline are known. Elevations near the shoreline produced by tsunamis with various return periods are known for the entire coastline of the Hawaiian Islands (except the coast of the uninhabited U. S. Navy target island of Kahoolawe) from Reference 19. As an example of the use of the numerical model, the model was applied to the Hauula-Punaluu region of the Island of Oahu (Figure 9) to determine flooding produced by 50- and 100-year tsunamis.

51. Topographic data and descriptions of vegetation covering the land for the Hauula-Punaluu region were taken from a flood hazard map of the region published by the State of Hawaii in cooperation with the

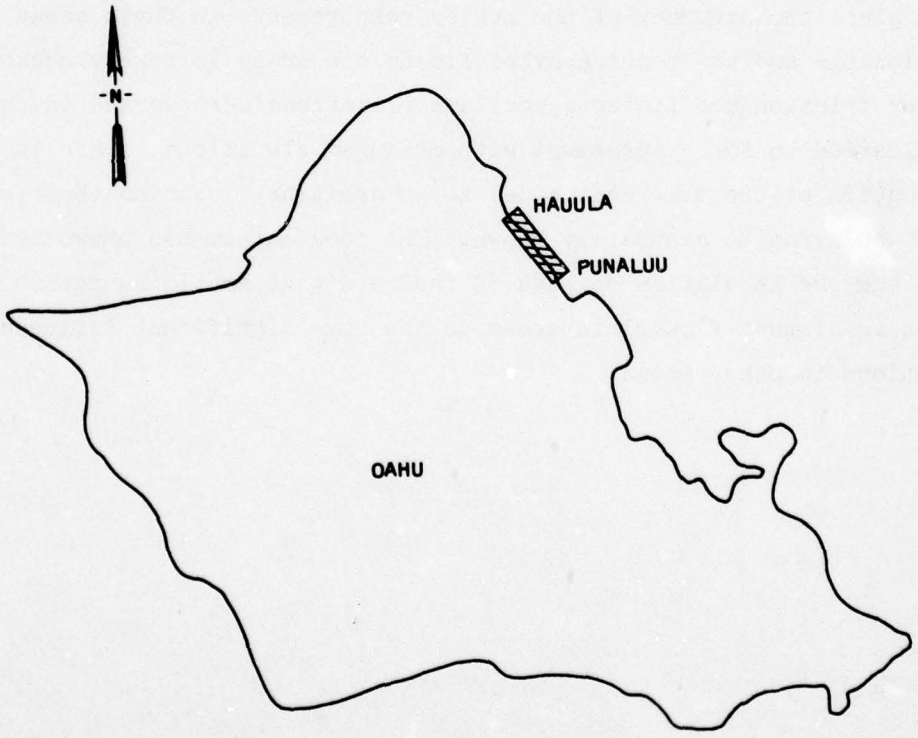

Figure 9. Location map for Hauula-Punaluu region

POD.[32] This map has a scale of 1:4800. Bathymetric data for the region were taken from the Hauula and Kahana quadrangle maps of the U. S. Geological Survey (scale of 1:24,000).

Numerical Grid and Boundary Conditions

52. Figure 10 shows the numerical grid used in the simulation of tsunami inundation in the Hauula-Punaluu region. The grid is oriented such that the incident wave approaches the Hauula-Punaluu region from a direction perpendicular to the 60-ft (mllw) bathymetric contour. It was assumed that refraction effects beyond the 60-ft contour bend the propagation path of a tsunami such that it approaches the nearshore area moving in a direction approximately perpendicular to this contour. The ocean bathymetry is reproduced out to the 60-ft contour (mllw) and beyond this contour the ocean is assumed to be a constant 60-ft depth (mllw).

53. The sizes of the grid cells in the region that is above msl were selected to allow a good representation of the land topography. Cells are longer in the direction approximately parallel to shoreline than in the direction perpendicular to it since land elevations vary more gradually in a direction parallel to the shoreline (land contours are approximately parallel to the shoreline). Cell sizes in the nearshore ocean region were selected for the same reason.

54. The input to the numerical model is a wave that when propagated to shore reproduces desired elevations 200 ft inland from shoreline at sites in Hauula and Punaluu. A distance of 200 ft inland from the shoreline was selected since the elevations presented in Reference 19 were based upon historical data recorded approximately 200 ft inland (on the average). Locations of these two sites are presented in Reference 33. Flooding was determined for elevations that are equaled or exceeded once in 100 years and once in 50 years at the two sites. Reference 19 predicts 100- and 50-year elevations of 12.6 and 9.7 ft, respectively, at Hauula and 13.0 and 10.4 ft, respectively, at Punaluu.

55. A trial-and-error method is used to produce desired elevations

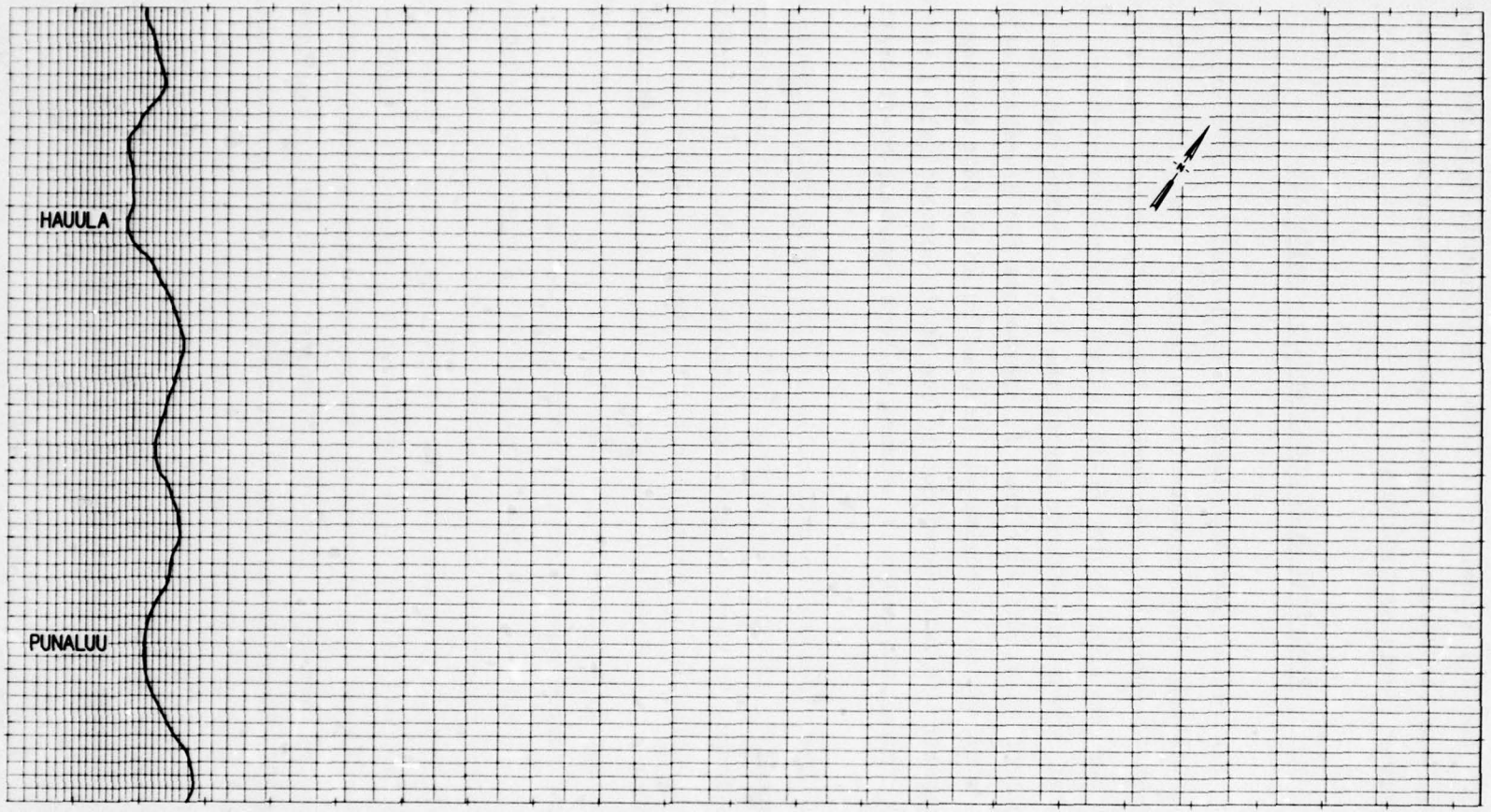

Figure 10. Numerical grid for Hauula-Punaluu region

at the Hauula and Punaluu sites. Different incident waves are tested until maximum elevations attain desired values at locations that are 200 ft inland from these two sites. The numerical model allows the incident wave form to vary along the input boundary. However, the great distance between the input boundary and the shoreline that was selected in order to eliminate the problem of reflected waves allows enough time during propagation for energy to move along the wave front and reduce the variability. To alleviate this problem it was necessary to add a thin nonpermeable barrier between the two sites that extended from the input boundary along the length of the constant depth region. This method allows an input boundary to be located in effect near the shoreline without the problem of reflected waves striking the true input boundary. Since the barrier is parallel to the direction of propagation of the tsunami, it does not create a problem by reflecting waves back toward the shoreline.

56. There were seven different Manning's n values used to represent frictional effects in the Hauula-Punaluu region. The ocean bottom and beaches were assigned a Manning's n equal to 0.024. Developed areas were assigned a Manning's n of 0.35, bush- and tree-covered areas or rough floodplain areas a value of 0.055, cultivated areas or floodplain areas without bushes and trees a value of 0.045, marsh areas a value of 0.040, reefs a value of 0.150, and noncultivated areas without bushes and trees a value of 0.030.

Results

57. Figures 11-20 show contours of 50- and 100-year tsunami inundations calculated using the numerical model for the Hauula-Punaluu region extending from Kaipapau Point to Makalii Point. The figures have the same scale as the map referenced[32] in the introduction to PART IV of this report. Thus the figures may be overlaid on this map to delineate detailed extents of inundation.

58. Inundation contours were determined first by delineating cells in the land area that were flooded during a part of the tsunami

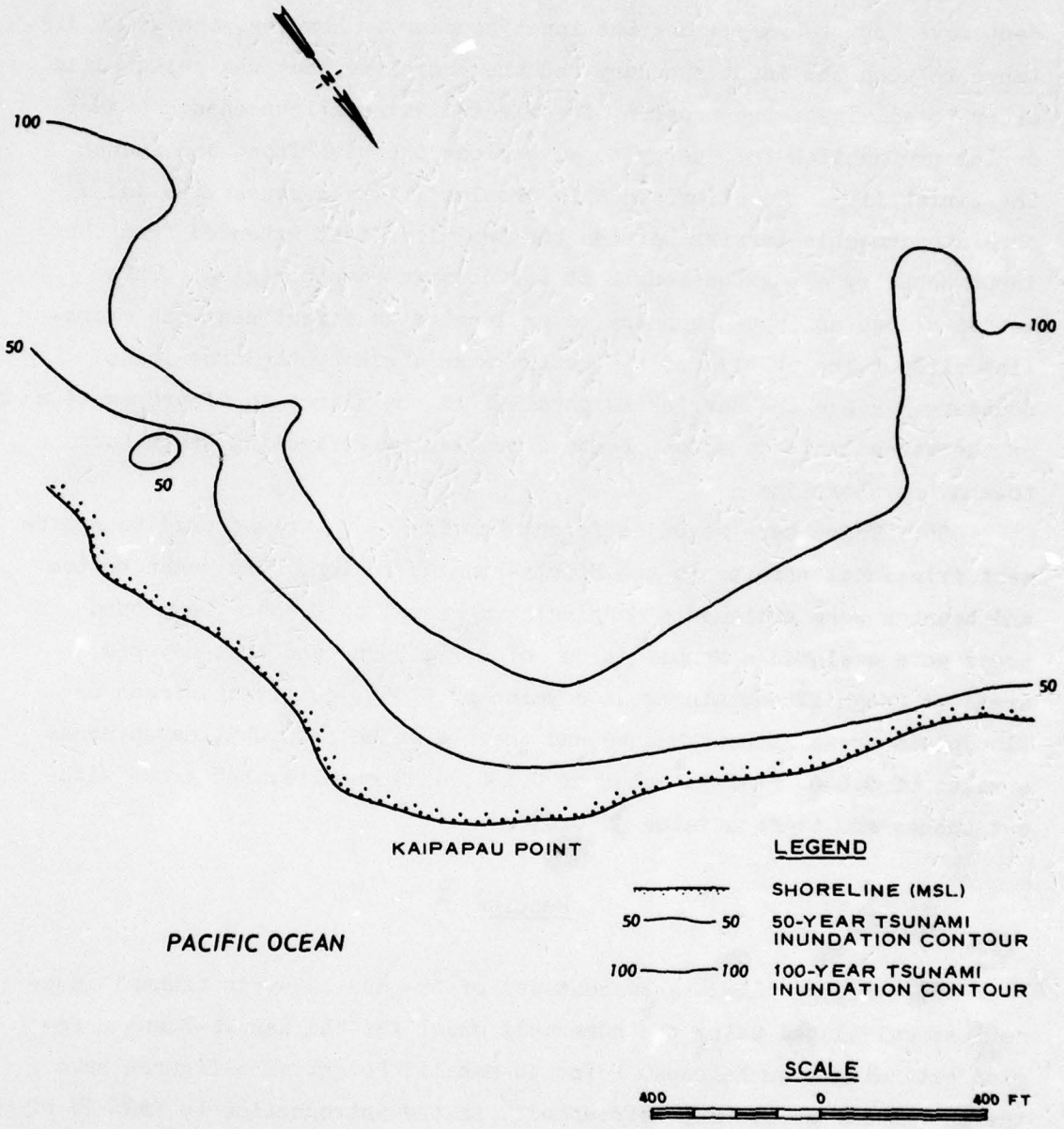

Figure 11. Tsunami inundation in the vicinity of Kaipapau Point

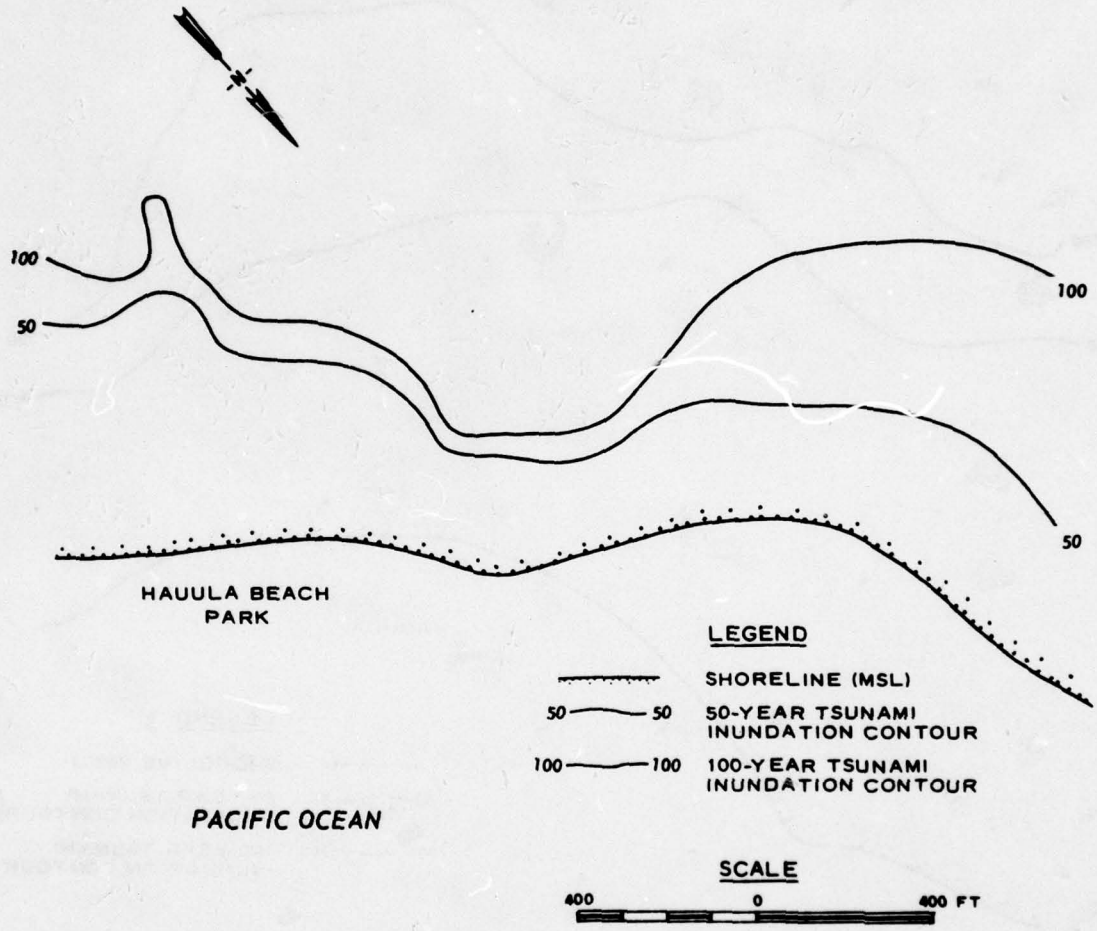

Figure 12. Tsunami inundation in the vicinity of Hauula Beach Park

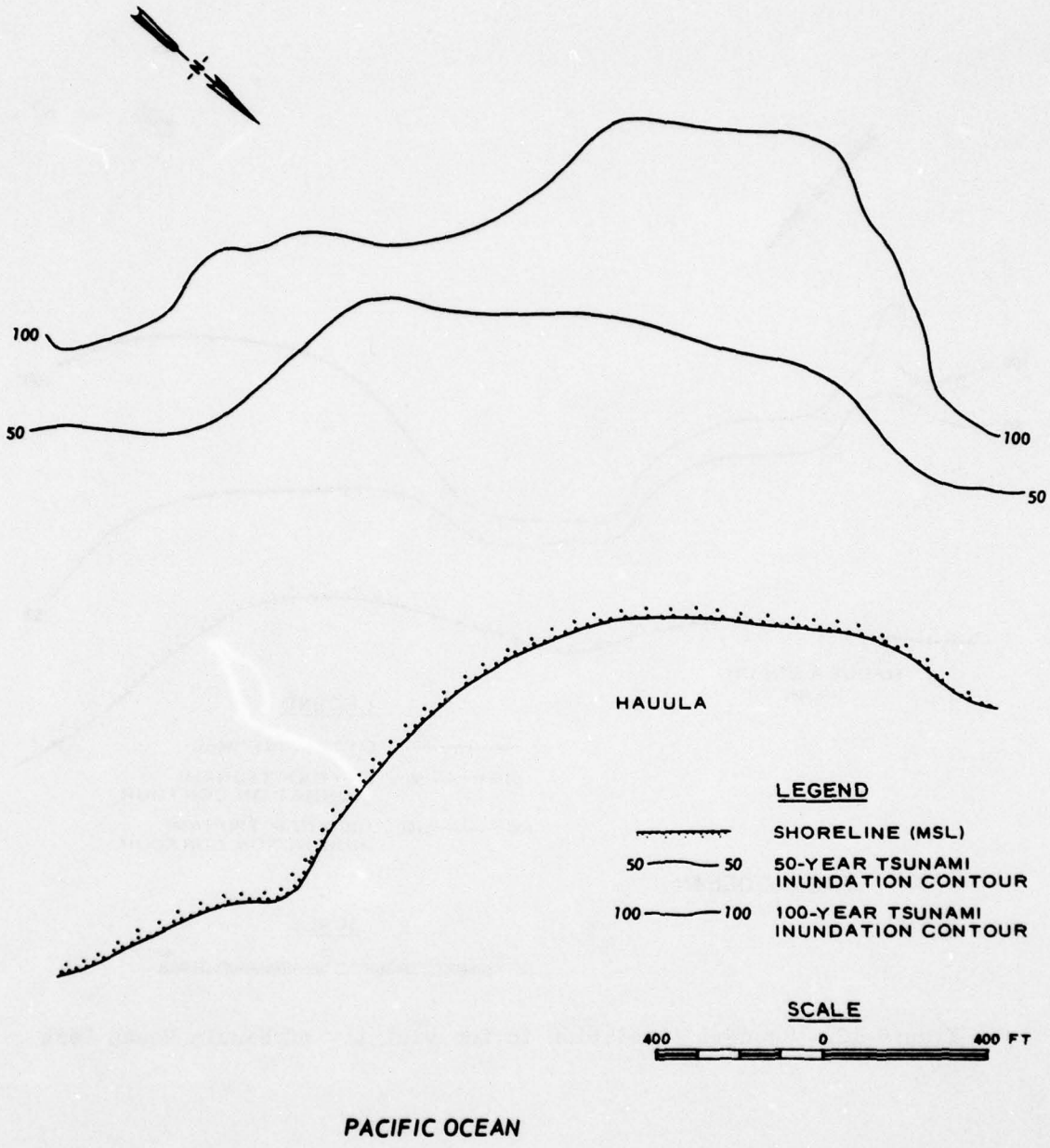

Figure 13. Tsunami inundation in the vicinity of Hauula

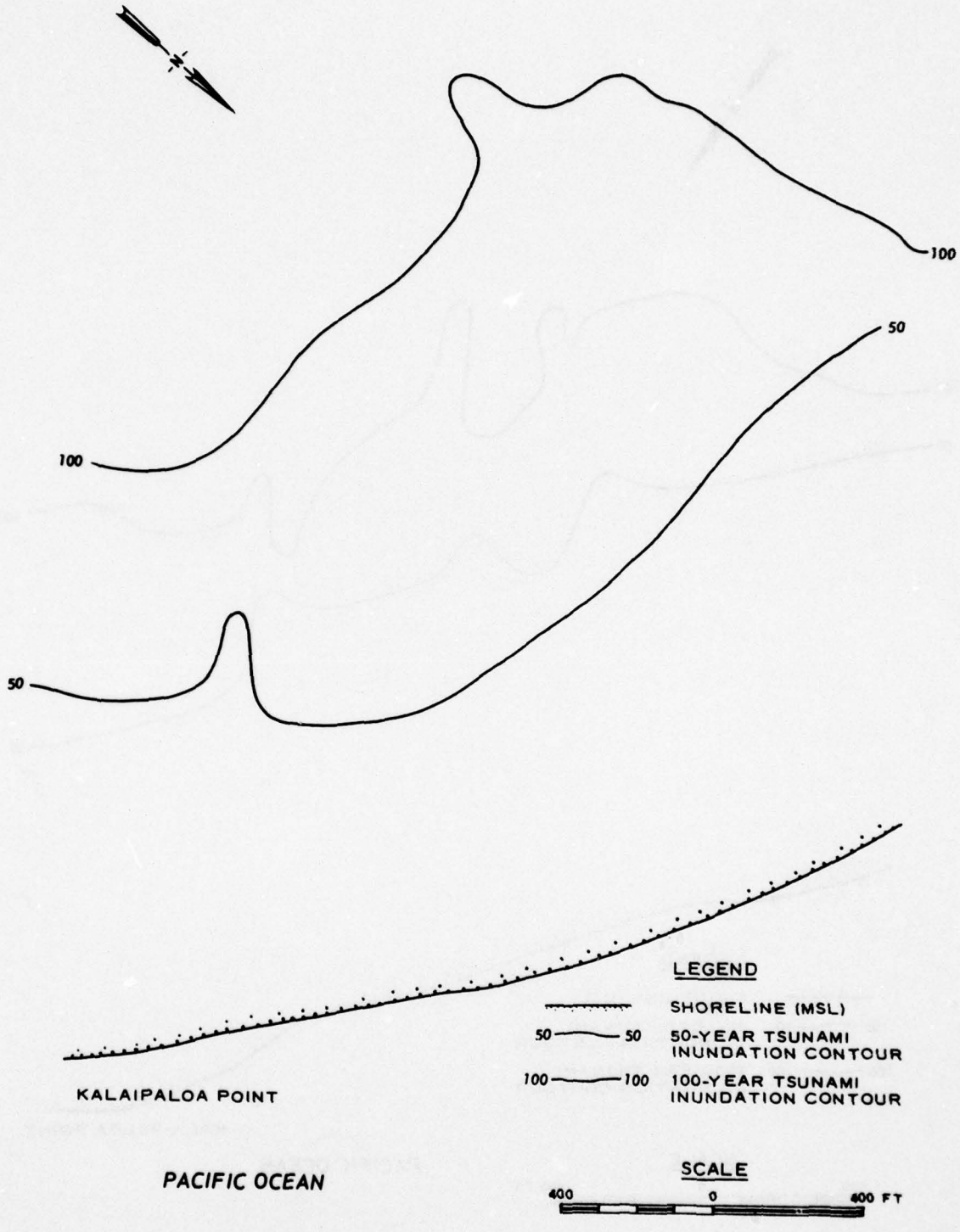

Figure 14. Tsunami inundation west of Kalaipaloa Point

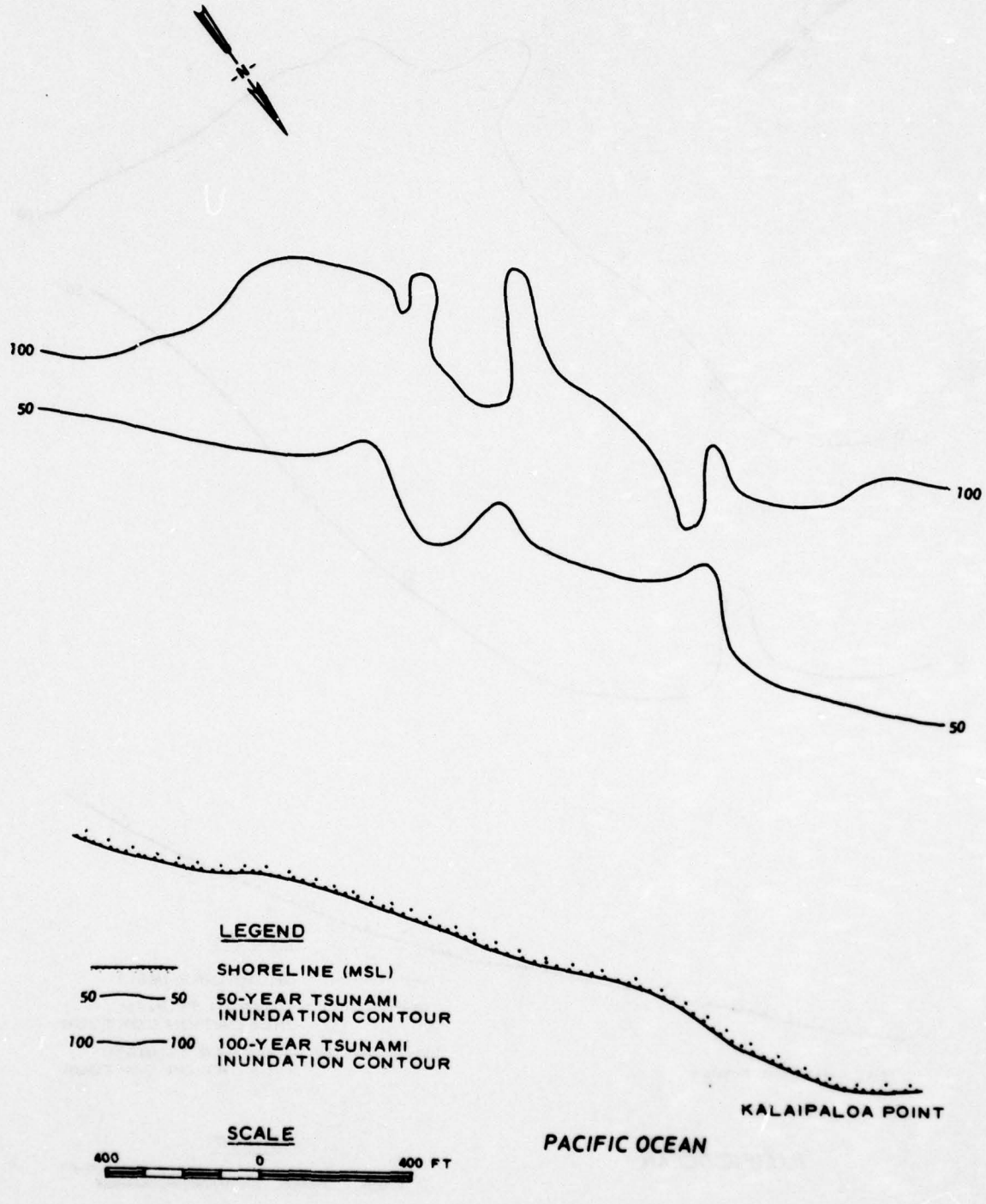

Figure 15. Tsunami inundation east of Kalaipaloa Point

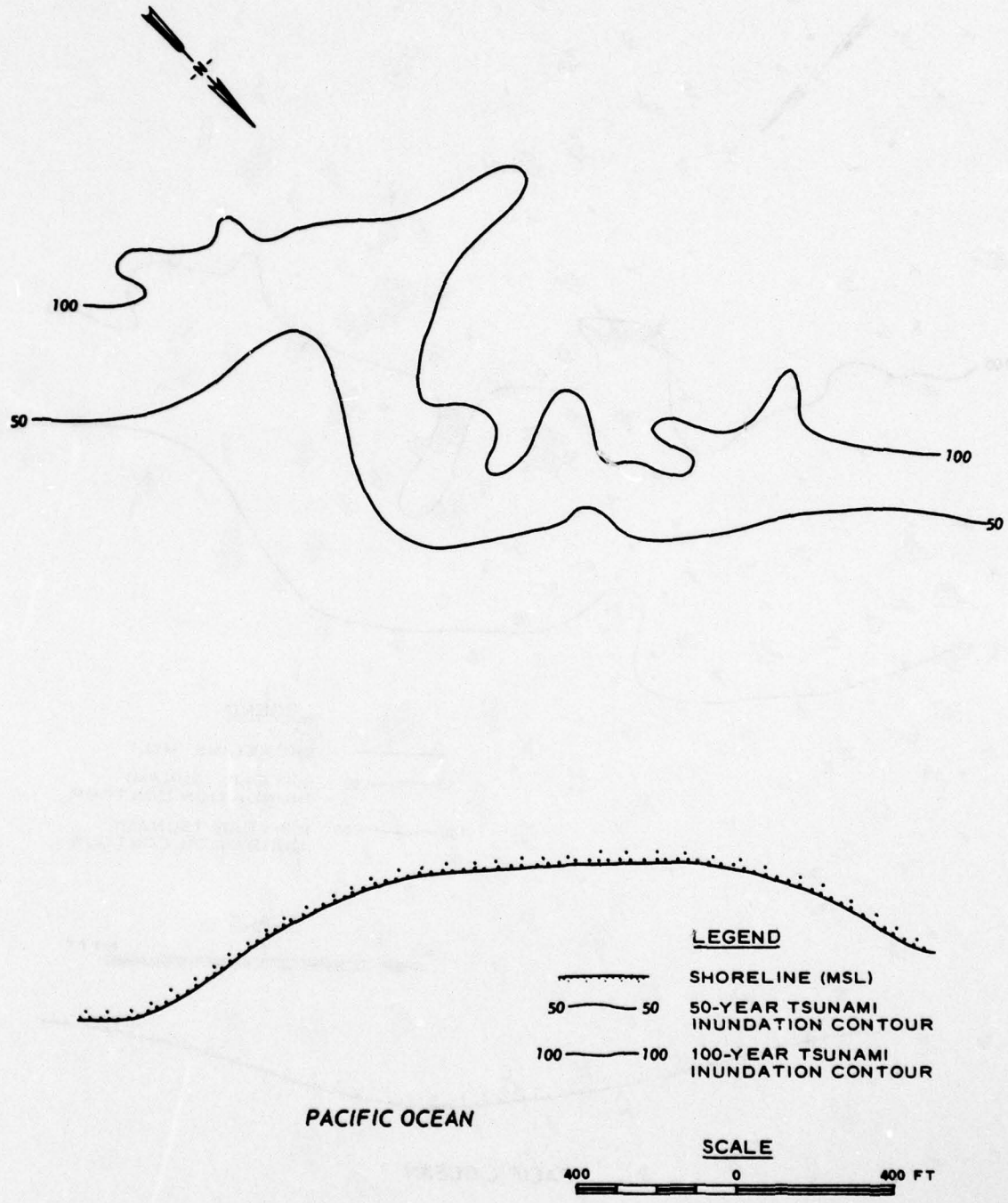

Figure 16. Tsunami inundation south of Kaluanui Stream

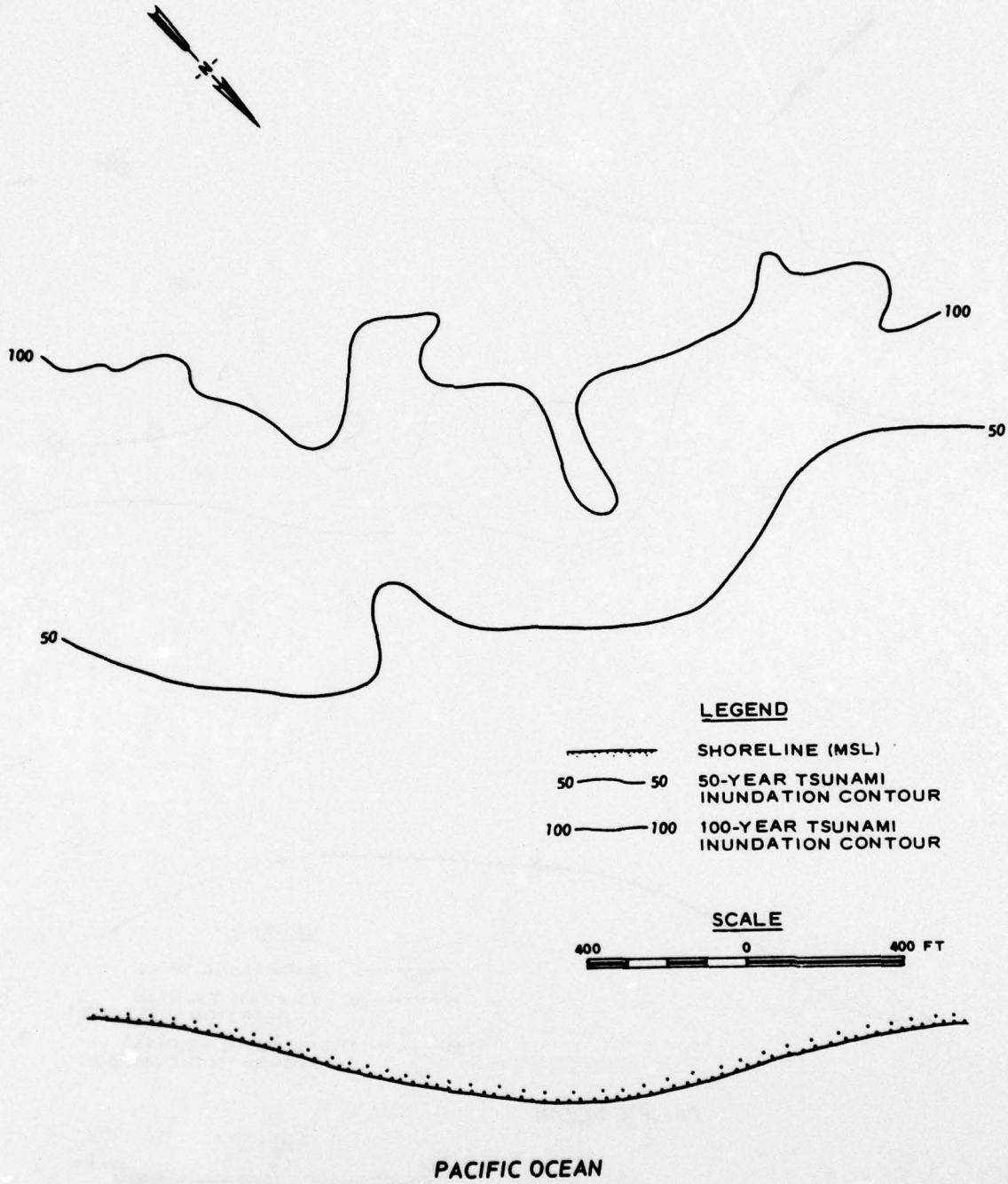

Figure 17. Tsunami inundation in the vicinity of Papaakuko

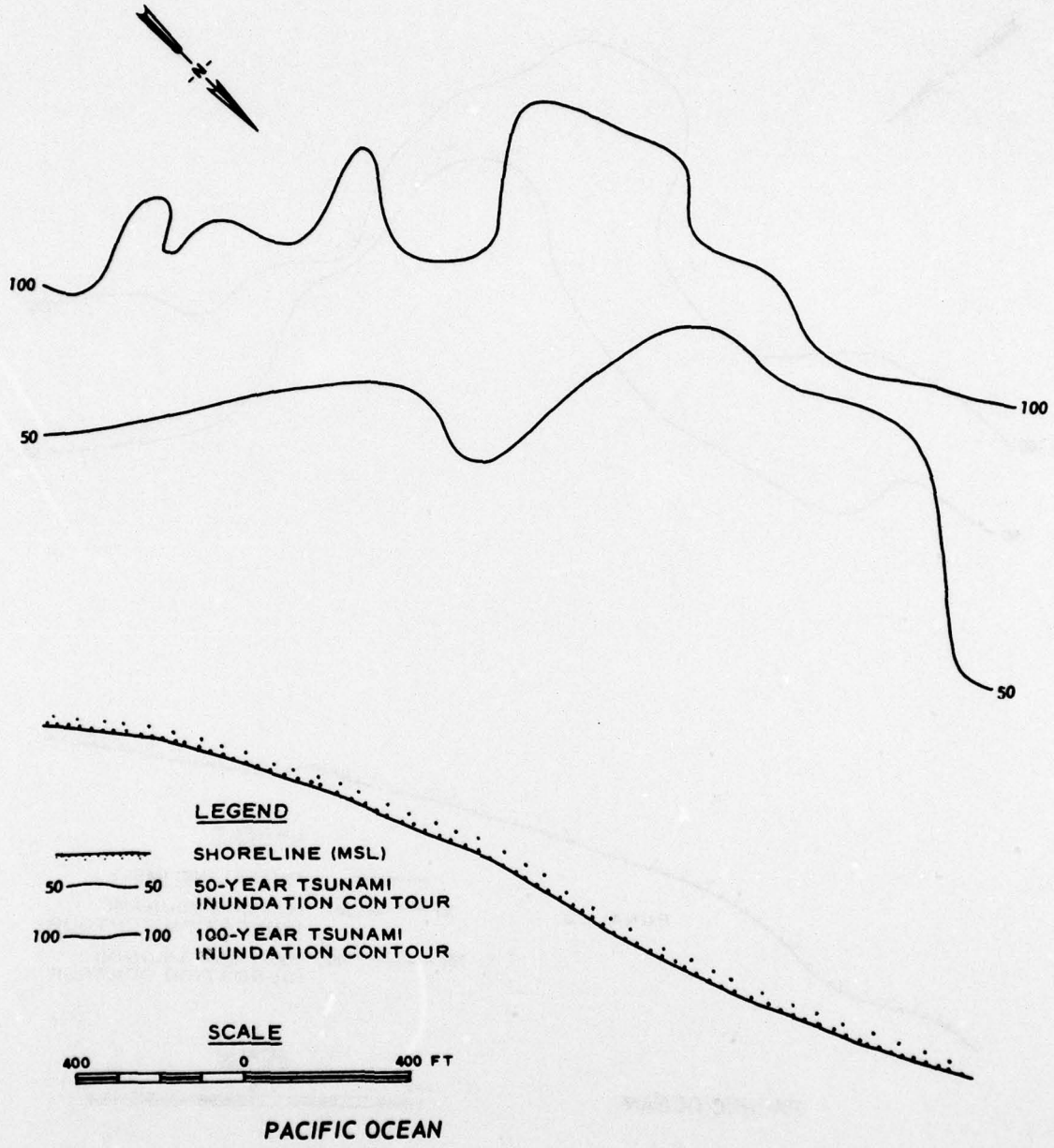

Figure 18. Tsunami inundation north of Punaluu

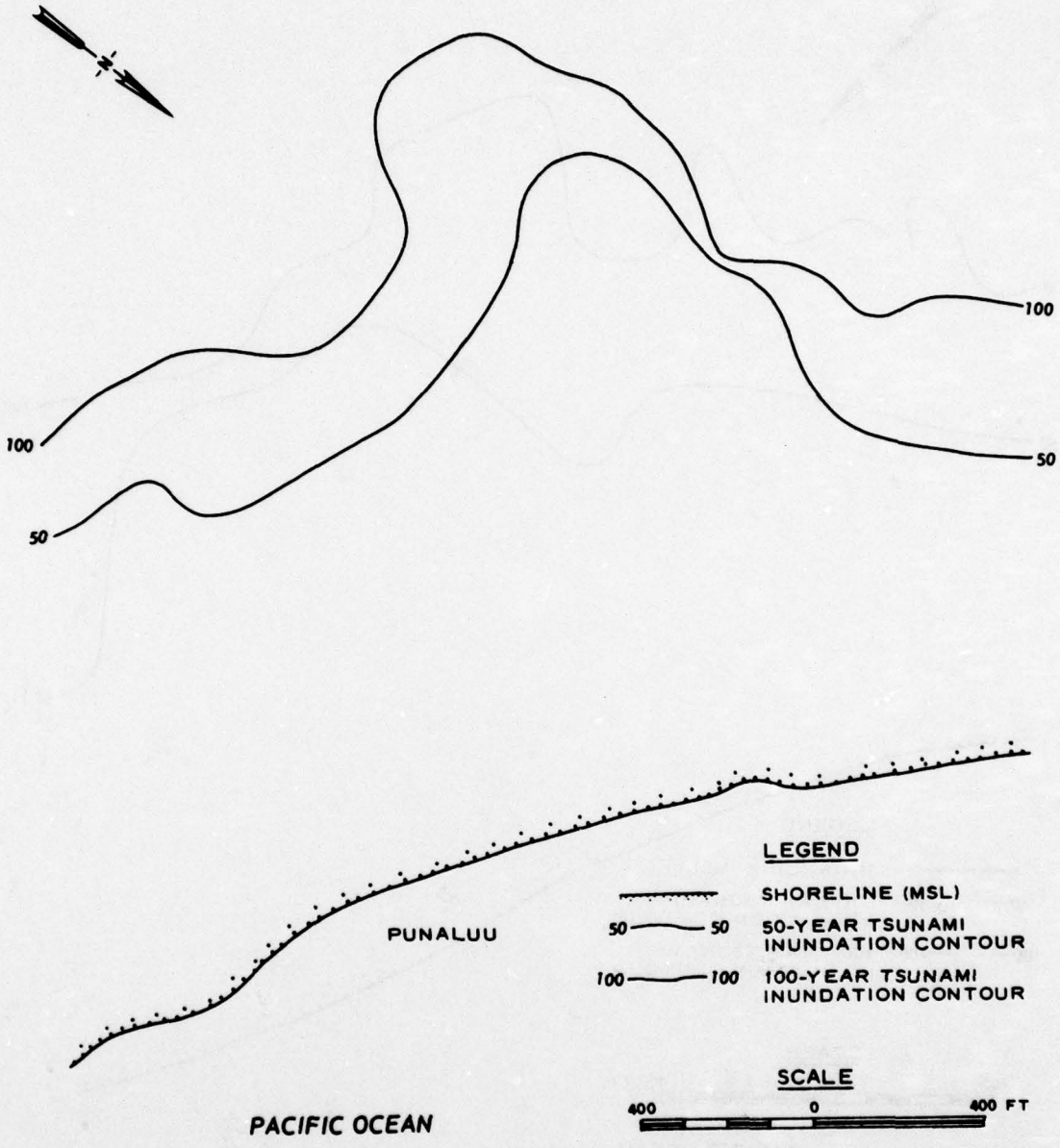

Figure 19. Tsunami inundation in the vicinity of Punaluu

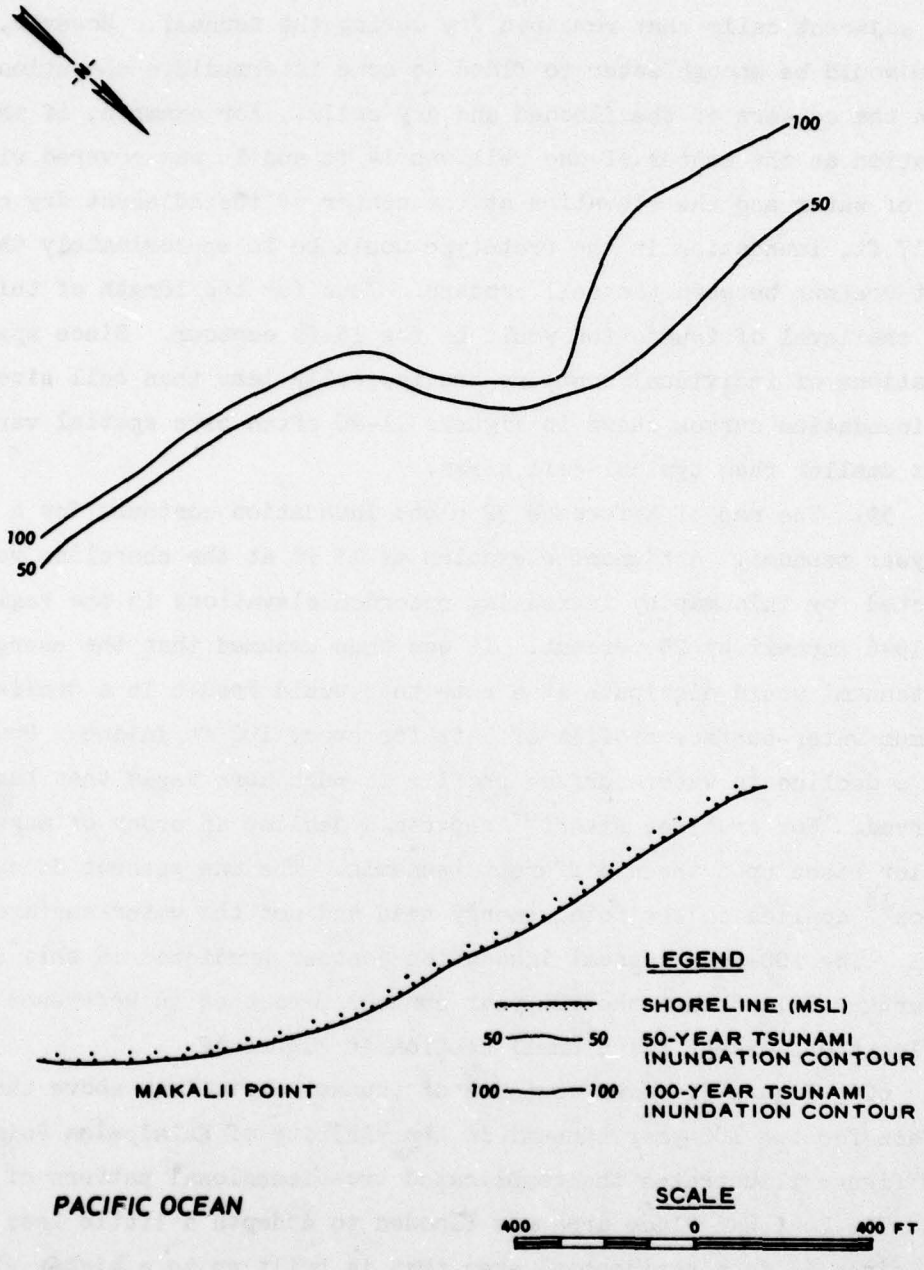

Figure 20. Tsunami inundation in the vicinity of Makalii Point

and also bordered cells that did not flood. These cells that did flood would have depths of water upon them that were not great enough to flood onto adjacent cells that remained dry during the tsunami. However, there would be enough water to flood to some intermediate elevation between the centers of the flooded and dry cells. For example, if the elevation at the center of one cell was 14 ft and it was covered with 1 ft of water and the elevation at the center of the adjacent dry cell was 17 ft, inundation in the prototype would be to approximately the 15-ft contour between the cell centers. Thus for the length of this cell the level of inundation would be the 15-ft contour. Since spatial variations of individual contours are typically less than cell sizes, the inundation curves shown in Figures 11-20 often have spatial variations smaller than typical cell sizes.

59. The map of Reference 32 plots inundation contours for a 100-year tsunami. A tsunami elevation of 15 ft at the shoreline was selected for this map by increasing recorded elevations in the region for the 1946 tsunami by 25 percent. It was then assumed that the energy of the tsunami would dissipate at a rate that would result in a declining maximum water-surface profile of 1 ft for every 100 ft inland. However, such a decline in water-surface profile is much more rapid than has been observed. For example, Hatori[34] reports a decline an order of magnitude smaller based upon three different tsunamis. The one percent decay used by Cox[15] applies to the total energy head and not the water-surface level. The 100-year tsunami inundation contour predicted in this study is farther inland than the 100-year contour presented in Reference 32 at all locations except for a small section in Figure 12.

60. Figure 21 shows contours of tsunami elevations above the land surface for the 100-year tsunami in the vicinity of Kalaipaloa Point. This figure illustrates the complicated two-dimensional pattern of flooding. The Poki Wai Place area was flooded to a depth a little less than 6 ft since it is a residential area that is built up to a higher elevation than neighboring land. Poki Wai Place is surrounded by a canal filled with water.

61. The numerical model predicts some interesting elevation

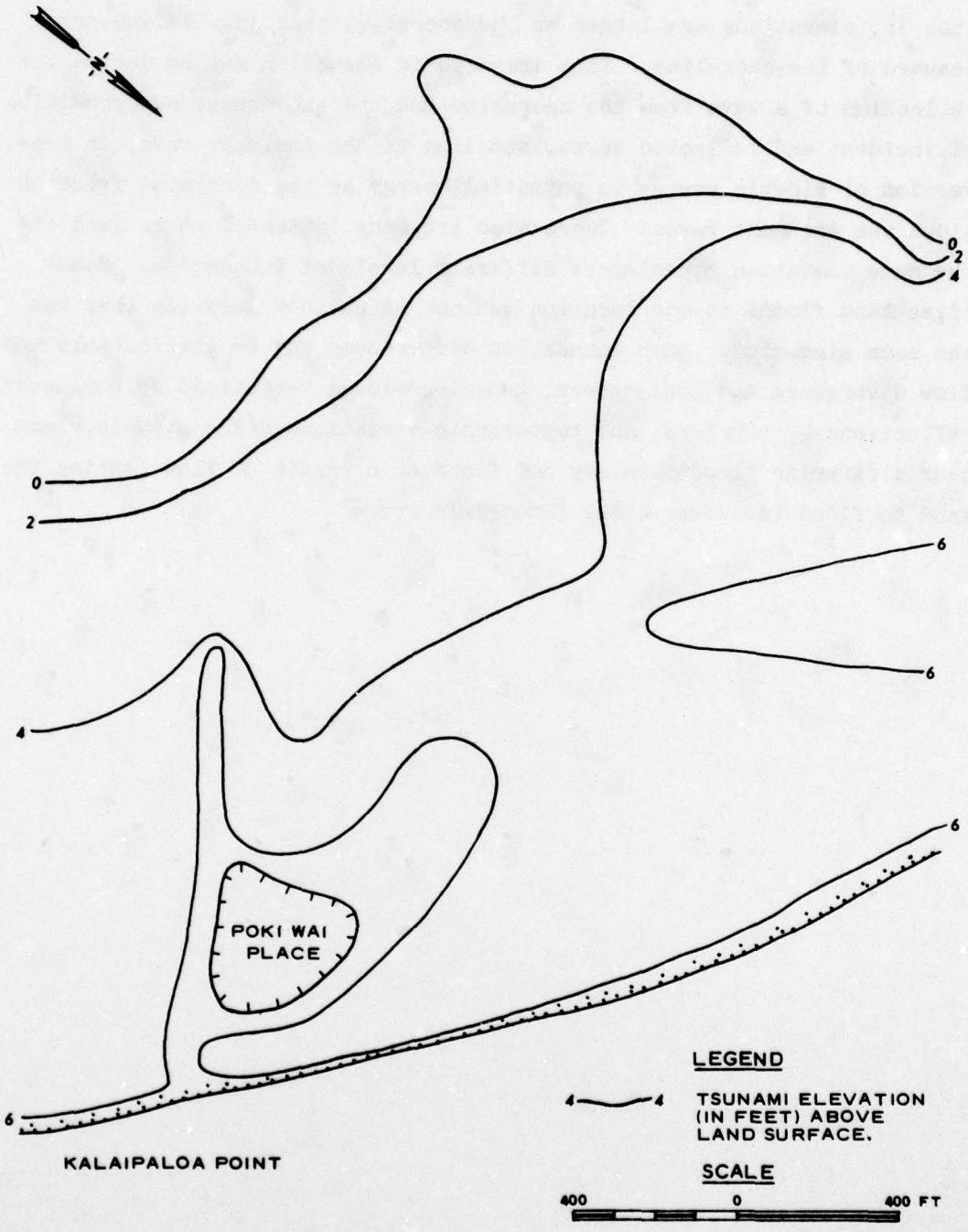

Figure 21. Tsunami elevations above the land surface

patterns. For example, at the shoreline there is an elevation "hump," that is, elevations are larger at the shoreline than just inland or seaward of the shoreline. This increase in elevation may be due to the reflection of a wave from the shoreline and the subsequent superposition of incident and reflected waves, shoaling of the incident wave, or conversion of kinetic energy to potential energy as the increased friction slows the incident waves. There also are many instances where land at the same elevation experiences different levels of inundation. Sometimes land floods at one location but not at another location that has the same elevation. Such inundation differences may be attributable to flow divergence and convergence, two-dimensional variations in roughness, reflections by barriers, and topographic variations. For example, land near a riverine floodplain may not flood as a result of flow passing the land to flood the lower lying floodplain area.

PART V: CONCLUSIONS

62. The finite difference numerical model presented in this report accurately predicts tsunami high-water marks and inundation for nonbore tsunamis. The model simulates two-dimensional, time-dependent, and dissipative effects. A conformal coordinate transformation allows the grid to be variable so that small grid cells can be concentrated in areas where high resolution is required. The grid cells can be large in the ocean region where high resolution is not necessary, since bathymetric variations are gradual and tsunami wavelengths are long. The variable grid makes it feasible to calculate tsunami inundation over a large area since it is not necessary to use very small grid cells over the entire region.

63. The tsunami inundation numerical model was developed to be quite general so that it could be used to predict tsunami flooding at arbitrary locations. The model allows nonpermeable breakwaters, permeable breakwaters, dynamic overtopping breakwaters, elevated roads, sand dunes, and other overtopping barriers. Frictional dissipation, land topography, and the ocean bathymetry can vary in any arbitrary two-dimensional fashion. Since tsunamis do not usually appear as bores, the model is applicable to most tsunami inundation problems. There also is evidence[1,5,7] that inundation produced by bores is similar to inundation produced by nonbores.

64. The numerical model presented in this report is an engineering tool that the POD can use to determine tsunami inundation throughout the Hawaiian Islands. The model has been documented in a separate WES report.[35]

REFERENCES

1. Wilson, B. W. and Tørum, A., "The Tsunami of the Alaskan Earthquake, 1964: Engineering Evaluation," Technical Memorandum No. 25, May 1968, U. S. Army Coastal Engineering Research Center, CE, Washington, D. C.

2. Pararas-Carayannis, G., "Catalog of Tsunamis in Hawaii," Report SE-4, Mar 1977, World Data Center A for Solid Earth Geophysics, Boulder, Colo.

3. U. S. Army Engineer District, Honolulu, CE, "The Tsunami of 23 May 1960 in Hawaii," Final Post Flood Report, 25 Apr 1962, Honolulu, Hawaii.

4. Magoon, O. T., "Structural Damage by Tsunamis," Coastal Engineering Santa Barbara Specialty Conference of the Waterways and Harbors Division, American Society of Civil Engineers, Oct 1965, pp 35-68.

5. Brown, D. L., "Tsunami Activity Accompanying the Alaskan Earthquake, 27 March 1964," Apr 1964, U. S. Army Engineer District, Alaska, CE, Anchorage, Alaska.

6. Nasu, N., "Heights of Tsunamis and Damage to Structures," Bulletin of the Earthquake Research Institute, Supplementary Volume 1, Tokyo Imperial University, 1934, pp 218-235.

7. Eaton, J. P., Richter, D. H., and Ault, W. V., "The Tsunami of May 23, 1960, on the Island of Hawaii," Bulletin of the Seismological Society of America, Vol 51, No. 2, Apr 1964, pp 135-157.

8. Palmer, R. Q., Mulvihill, M. E., and Funasaki, G. T., "Hilo Harbor Tsunami Model--Reflected Waves Superimposed," Coastal Engineering Santa Barbara Specialty Conference of the Waterways and Harbors Division, American Society of Civil Engineers, Oct 1965, pp 21-31.

9. Senter, P. K., "Design of Proposed Crescent City Harbor, California, Tsunami Model," Technical Report H-71-2, U. S. Army Engineer Waterways Experiment Station, CE, Vicksburg, Miss.

10. Freeman, J. C. and LeMehaute, B., "Wave Breakers on a Beach and Surges on a Dry Bed," Journal of the Hydraulics Division, American Society of Civil Engineers, Mar 1964, pp 187-216.

11. Kishi, T. and Saeki, H., "The Shoaling, Breaking and Runup of the Solitary Wave on Impermeable Rough Slopes," Proceedings of the Tenth Conference on Coastal Engineering, Tokyo, Japan, Chapter 21, Sep 1966.

12. Spielvogel, L. Q., "Single-Wave Runup on Sloping Beaches," Journal of Fluid Mechanics, Vol 74, Part 4, 1975, pp 685-694.

13. Heitner, K. L. and Housner, G. W., "Numerical Model for Tsunami Run-Up," Journal of the Waterways, Harbor and Coastal Division, American Society of Civil Engineers, Aug 1970, pp 701-719.

14. Bretschneider, C. L. and Wybro, P. G., "Tsunami Inundation Prediction," Proceedings of the 15th Coastal Engineering Conference, American Society of Civil Engineers, pp 1000-1024.

15. Cox, D. C., "Potential Tsunami Inundation Areas in Hawaii," Report No. 14, 1961, Hawaii Institute of Geophysics.

16. Reid, R. O. and Bodine, B. R., "Numerical Model for Storm Surges in Galveston Bay," Journal of the Waterways and Harbors Division, American Society of Civil Engineers, Vol 94, No. WWI, Feb 1968.

17. Masch, F. D., Brandes, R. J., and Reagan, J. D., "Simulation of Hydrodynamics in a Tidal Inlet," 1973, Water Resources Engineers, Inc., Austin, Tex.

18. Butler, H. L., "Numerical Simulation of Tidal Hydrodynamics, Great Egg Harbor and Corson Inlets, New Jersey," Technical Report H-78-11, 1978, U. S. Army Engineer Waterways Experiment Station, CE, Vicksburg, Miss.

19. Houston, J. R., Carver, R. D., and Markle, D. G., "Tsunami-Wave Elevation Frequency of Occurrence for the Hawaiian Islands," Technical Report H-77-16, 1977, U. S. Army Engineer Waterways Experiment Station, CE, Vicksburg, Miss.

20. Lamb, H., Hydrodynamics, Cambridge University Press, London, England, 1932.

21. Dronkers, J. J., Tidal Computations in Rivers and Coastal Waters, North-Holland Publishing Co., Amsterdam, 1964.

22. Leendertse, J. J., "Aspects of a Computational Model for Long-Period Water-Wave Propagation," Memorandum RM-5294-PR, May 1967, The Rand Corporation, Santa Monica, Calif.

23. Wang, J. D. and Connor, J. J., "Mathematical Modeling of Near Coastal Circulation," Report No. 200, Apr 1975, Ralph M. Parsons Laboratory, Massachusetts Institute of Technology, Cambridge, Mass.

24. Wanstrath, J. J., "Nearshore Numerical Storm Surge and Tidal Simulation," Technical Report H-77-17, 1977, U. S. Army Engineer Waterways Experiment Station, CE, Vicksburg, Miss.

25. _____, "Storm Surge Simulation in Transformed Coordinates; Vol 1: Theory and Application," Technical Report 76-3, U. S. Coastal Engineering Research Center, Fort Belvoir, Va.

26. Wiegel, R. L., Oceanographical Engineering, Prentice-Hall, Inc., Englewood Cliffs, N. J., 1964.

27. Wiegel, R. L., "Protection of Crescent City, California, from Tsunami Waves," 1965, The Redevelopment Agency of the City of Crescent City, Berkeley, Calif.

28. Roberts, J. A. and Kauper, E. K., "The Effects of Wind and Precipitation on the Modification of South Beach, Crescent City, California," ARG64 FR-186, 1964, Office of the Chief of Research and Development, Washington, D. C.

29. Keulegan, G. H., Harrison, J., and Mathews, M. J., "Theoretics in Design of the Proposed Crescent City Harbor Tsunami Model," Technical Report H-69-9, U. S. Army Engineer Waterways Experiment Station, CE, Vicksburg, Miss.

30. Creager, W. P. and Justin, J. D., Hydroelectric Handbook, 1950, Wiley, New York, N. Y.

31. Parsons, D. A., "Vegetative Control of Streambank Erosion," Proceedings, Federal Inter-Agency Sedimentation Conference Paper No. 20, pp 130-136, U. S. Government Printing Office, Washington, D. C.

32. Department of Land and Natural Resources of the State of Hawaii, "Hauula-Punaluu Flood Hazard Area," MAP FP-20, Nov 1973.

33. Loomis, H. G., "Tsunami Wave Runup Heights in Hawaii," HIG-76-5, May 1976, Hawaii Institute of Geophysics, University of Hawaii, Honolulu, Hawaii.

34. Hatori, T., "A Study of the Damage to Houses due to a Tsunami," Bulletin of the Earthquake Research Institute, University of Tokyo, Vol 42, 1964, pp 181-196.

35. Houston, J. R. and Butler, H. L., "User's Manual for Tsunami Inundation Numerical Model" (in preparation), U. S. Army Engineer Waterways Experiment Station, CE, Vicksburg, Miss.

APPENDIX A: NOTATION

a_1	Constant coefficient
a_2	Constant coefficient
a_m	Coefficient defined at location m
A_m	Variable defined at location m
b_1	Constant coefficient
b_2	Constant coefficient
B_m	Variable defined at location m
c_1	Constant coefficient
c_2	Constant coefficient
C	Chezy frictional coefficient
d	Total water depth, ft
d*	$\bar{\eta}^k - \bar{h}$, averaged total water depth, ft
$\hat{d}$	$\bar{\eta}^{k+1/2} - \bar{h}$, averaged total water depth, ft
Dl	Variable
g	Acceleration due to gravity, 32.2 ft/sec^2
h	Still-water depth, ft
k	Integral associated with time levels
L	Integral grid index
m	Integral grid index
M	Integral grid index
n	Integral grid index
n_m	Manning's n
P_m	Variable defined at grid index m
Q_m	Variable defined at grid index m
R_m	Variable defined at grid index m
S_m	Variable defined at grid index m
t	Time, sec
Δt	Time-step for completing two cycles, sec
Tl	Variable
T2	Variable
U	Vertically integrated transport per unit width in x-direction, ft^2/sec

V	Vertically integrated transport per unit width in y-direction, ft^2/sec
x	Cartesian coordinate, ft
y	Cartesian coordinate, ft
α_1	Coordinate in computational space
α_2	Coordinate in computational space
η	Water-surface elevation, ft
μ_1	Variable defining stretching of computational grid
μ_2	Variable defining stretching of computational grid
τ	Time-step for completing one cycle, sec
$-$	Two-point time average when over variable
$=$	Four-point time average when over variable

In accordance with letter from DAEN-RDC, DAEN-ASI dated 22 July 1977, Subject: Facsimile Catalog Cards for Laboratory Technical Publications, a facsimile catalog card in Library of Congress MARC format is reproduced below.

Houston, James R
A numerical model for tsunami inundation / by James R. Houston, H. Lee Butler. Vicksburg, Miss. : U. S. Waterways Experiment Station ; Springfield, Va. : available from National Technical Information Service, 1979.
54, 2 p. : ill. ; 27 cm. (Technical report - U. S. Army Engineer Waterways Experiment Station ; HL-79-2)
Prepared for U. S. Army Engineer Division, Pacific Ocean, Fort Shafter, Hawaii.
References: p. 52-54.

1. Floods. 2. Long waves. 3. Mathematical models. 4. Tsunamis. I. Butler, H. Lee, joint author. II. United States. Army. Corps of Engineers. Pacific Ocean Division. III. Series: United States. Waterways Experiment Station, Vicksburg, Miss. Technical report ; HL-79-2.
TA7.W34 no.HL-79-2